1    **Mapping Global Non-Floodplain Wetlands**

3    Charles R. Lane[1], Ellen D'Amico[2], Jay R. Christensen[3,★], Heather E. Golden[3,★], Qiusheng Wu[4], and

4    Adnan Rajib[5]

6    [1] U.S. Environmental Protection Agency, Office of Research and Development, Center for Environmental

7         Measurement and Modeling, Athens, Georgia, United States of America

8    [2] Pegasus Corporation c/o U.S. Environmental Protection Agency, Office of Research and Development,

9         Cincinnati, Ohio, United States of America

10   [3] U.S. Environmental Protection Agency, Office of Research and Development, Center for Environmental

11        Measurement and Modeling, Cincinnati, Ohio, United States of America

12   [4] Department of Geography & Sustainability, University of Tennessee, Knoxville, Tennessee, United

13        States of America

14   [5] Hydrology and Hydroinformatics Innovation Lab, Department of ~~Environmental~~ Civil Engineering,

15        ~~Texas A&M University~~University of Texas at Arlington, ~~Kingsville~~Arlington, Texas, United States

16        of America

18   ★ These authors contributed equally to this work

20   **Correspondence:** Charles Lane (lane.charles@epa.gov) and Ellen D'Amico (damico.ellen@epa.gov)

22   **Abstract.** Non-floodplain wetlands – those located outside the floodplains – have emerged as integral

23   components to watershed resilience, contributing hydrologic and biogeochemical functions affecting

24   watershed-scale flooding extent, drought magnitude, and water-quality maintenance. However, the

25   absence of a global dataset of non-floodplain wetlands limits their necessary incorporation into water

26  quality and quantity management decisions and affects wetland-focused wildlife habitat conservation

27  outcomes. We addressed this critical need by developing a publicly available Global NFW (non-

28  floodplain wetland) dataset, comprised of a global river-floodplain map at 90 m resolution coupled with a

29  global ensemble wetland map incorporating multiple wetland-focused data layers. The floodplain,

30  wetland, and non-floodplain wetland spatial data developed here were successfully validated within 21

31  large and heterogenous basins across the conterminous United States. We identified nearly 33 million

32  potential non-floodplain wetlands with an estimated global extent of over 16 million km$^2$. Non-floodplain

33  wetland pixels comprised 53% of globally identified wetland pixels, meaning the majority of the globe's

34  wetlands likely occur external to river floodplains and coastal habitats. The identified Global NFWs were

35  typically small (median 0.039 km$^2$), with a global median size ranging from 0.018-0.138 km$^2$. This novel

36  geospatial Global NFW static dataset advances wetland conservation and resource-management goals

37  while providing a foundation for global non-floodplain wetland functional assessments, facilitating non-

38  floodplain wetland inclusion in hydrological, biogeochemical, and biological model development. The

39  data are freely available through the United States Environmental Protection Agency's Environmental

40  Dataset Gateway (https://gaftp.epa.gov/EPADataCommons/ORD/Global_NonFloodplain_Wetlands/) and

41  through https://doi.org/10.23719/1528331 (Lane et al., 2023).

43  **1      Introduction**

45  Wetlands are recognized as globally important ecosystems providing functions leading to critical

46  provisioning (e.g., food, fresh water for domestic, agricultural, and industrial use) and regulating services

47  (e.g., flood and drought mitigation, water purification and waste treatment, and habitat; Millennium

48  Ecosystem Assessment, 2005). Despite their functional importance, wetlands are threatened worldwide by

49  myriad anthropogenic disturbances, including sea-level rise (IPCC, 2014), drainage and filling (Davidson

50  et al., 2014), water abstraction (Liu et al., 2017), consolidation (McCauley et al., 2015), invasive species

51  (Zedler and Kercher, 2004), and changing precipitation and temperature patterns (Winter, 2000). These

52  widespread and globally prevalent alterations to wetlands affect their functioning, resulting in increased

53  downgradient flooding (Golden et al., 2021), modified stream baseflows (Buttle, 2018), reduced pollution

54  mitigation (Evenson et al., 2018a), and habitat loss (Uden et al., 2015).

56  Watershed-scale wetland management is currently hampered by the paucity of accurate and fine-grained

57  maps of wetland location (Creed et al., 2017; Christensen et al., 2022). However, methods to identify

58  existing aquatic systems, including wetlands, that provide functions at global scales have recently

59  emerged, such as the Landsat-based 30 m global surface-water inundation data (Pekel et al., 2016), finer-

60  resolution satellite-based landcover maps (e.g., Zanaga et al., 2021), and groundwater-driven aquatic

61  system characterizations (Fan et al., 2013). In addition, methods utilizing digital elevation models to

62  identify topographic depressions likely to support aquatic systems with characteristic wetland features,

63  such as saturated soils and/or ponded waters, have also regionally proliferated (Wu et al., 2019a; Wu et

64  al., 2019b; Christensen et al., 2022).

66  These advancements in mapping wetland location, such as those located within the river floodplain or

67  geographically distal from floodplains, allow resource managers to better incorporate wetland

68  biogeochemical, hydrological, and biological functions and concomitantly ecosystem services into their

69  decision-making efforts. For instance, incorporating *floodplain* wetlands into decision-making advances

70  the wise management and conservation of mapped riparian ecosystems (Tullos, 2018; Kundzewicz et al.,

71  2018). Thus, recognizing the importance of wetlands located within active river floodplains, land-

72  management decisions are being made to quantify the functions and ecosystem services of these wetlands

73  and incorporate them into watershed-scale hydro-ecological decisions (e.g., Makungu and Hughes, 2021;

74  Rajib et al., 2021).

75

76  However, *non-floodplain wetlands* are typically not incorporated into watershed-scale conservation and

77  management planning (e.g., Sullivan et al., 2019), thereby ignoring their contributions to watershed-scale

78  resilience in response to biogeochemical and hydrological disturbances (Rains et al., 2016; Golden et al.,

79  2021; Lane et al., 2022). Non-floodplain wetlands are abundant inland freshwater wetlands located

80  distally from the floodplains of rivers and lakes (Lane and D'Amico, 2016; Lane et al., 2018). Though

81  typically small (Cohen et al., 2016), high biogeochemical processing rates within non-floodplain wetlands

82  have resulted in these systems being termed bioreactors (Marton et al., 2015). Indeed, a literature review

83  of over 600 articles found that the highest reactivity rates (pollutant mass removal per unit time) were

84  found in the smallest water bodies and wetlands (Cheng and Basu, 2017). Further, the high reactivity of

85  individual non-floodplain wetlands can cumulatively improve downgradient water quality conditions

86  (Golden et al., 2019; Evenson et al., 2021). Non-floodplain wetlands may therefore have an outsized

87  impact on a watershed's water quality.

88

89  Non-floodplain wetlands are also important ecosystems affecting water quantity (i.e., for storing and

90  gradually releasing water to downgradient rivers and streams). Specifically, precipitation is captured and

91  stored in non-floodplain wetlands prior to being discharged downgradient. During this storage period,

92  water can infiltrate to recharge aquifers, evaporate or transpire, or eventually "spill" overland and be

93  transported downstream (Jones et al., 2018; Buttle, 2018). These non-floodplain wetland water storage

94  functions attenuate storm flows (Shaw et al., 2012; Fossey and Rousseau, 2016; Blanchette et al., 2022)

95  and recharge groundwaters (Bam et al., 2020), thereby mitigating flood-hazards (Mclaughlin et al., 2014)

96  and ameliorating drought conditions by maintaining baseflow (Ameli and Creed, 2019).

97

98  Despite the important functions provided by non-floodplain wetlands (Biggs et al., 2017; Chen et al.,

99  2022) a substantive data gap remains: no global maps or datasets exist identifying the geospatial location

100  of non-floodplain wetlands and open waters. Regionally focused efforts, such as the recent work by Lane

101  and D'Amico (2016) and Lane et al. (2022) mapped the extent of non-floodplain wetlands (also known as

102  geographically isolated wetlands, Leibowitz, 2015; Mushet et al., 2015) across the geospatially data-rich

103  conterminous United States (CONUS, see abbreviation list in Appendix A). They found that 16-23 % of

104    freshwater systems were potential non-floodplain wetlands, suggesting a substantial yet hitherto unknown

105    portion of the globe's wetlands are likely also this vulnerable water resource.

106

107    Fortunately, geospatial data for identifying aquatic systems, including wetlands, are burgeoning (Khare et

108    al., in review). Global land cover and land use geospatial datasets that include a wetland cover class

109    continue to propagate (Hu et al., 2017a), taking advantage of both lengthy time-series Landsat data

110    (Homer et al., 2020) as well as recently launched advanced high-resolution and/or synthetic aperture radar

111    (SAR) equipped satellites (e.g., Sentinel-1, Sentinel-2, plus many commercially available platforms;

112    Martinis et al., 2022) and topographic data sources and analyses (e.g., Wu et al., 2019b). Examples

113    include the GlobeLand30 (Chen et al., 2015), the European Space Agency (ESA) WorldCover 2020

114    (ESA, 2020), the Dynamic World (Brown et al., 2022), as well as consortiums focusing on annual land

115    cover change mapping (e.g., Tsendbazar et al., 2021). Several recent publications review the available

116    wetland-focused datasets, including Hu et al. (2017a, their Table 1), Davidson et al. (2018, their Table

117    S1), Tootchi et al. (2019, their Table 1), and Zhang et al. (2023, their Table 1). We summarize additional

118    emerging global land cover data sets related to surface water and wetlands in Appendix Table B1.

119

120    Lehner and Döll (2004) were amongst the first to publish a geospatially explicit global map focusing on

121    wetland extents. Their Global Lakes and Wetlands Database provides 1 km estimates of wetland

122    abundance. More recent and/or higher resolution wetland-focused datasets have emerged, including the 1

123    km global dataset from Hu et al. (2017b) that incorporates precipitation and a topographic wetness index,

124    and the multi-sourced 500 m composite maps of regularly flooded and groundwater-driven wetlands by

125    Tootchi et al. (2019). Tootchi et al.'s (2019) approach identified small and scattered wetlands. However,

126    they recognized the limitations inherent in their global product (ca. 500 m per pixel resolution) resulted in

127    omission errors for many wetland systems, especially those smaller than their 500 x 500 m (25 ha) data

128    resolution. This suggests, and Tootchi et al. (2019) acknowledged, that many (non-floodplain) wetlands

129    were omitted in the Tootchi et al. (2019) 500 m global product. Cohen et al. (2016) determined non-

130 floodplain wetlands in the CONUS are "unambiguously small", e.g., their average non-floodplain wetland

131 area was just over two hectares (2.1 ha). Based on the "all or nothing" methodological approach in

132 Tootchi et al. (2019), > 12.5 ha of a given 25.0 ha cell [one homogenous pixel] cell would have to be

133 identified as wetland in their resampling of the finer-scale data – much larger than the average 2.1 ha

134 wetlands found in Cohen et al. (2016).

135

136 Concurrent with increasingly available global land cover and wetland data, there is an increasing global

137 focus on deriving floodplain and flood hazard- prone areal extents within river networks based on high-

138 resolution topographic data coupled with hydrologic and/or hydraulic modeling (Tullos, 2018;

139 Kundzewicz et al., 2018; Rajib et al., in review). The past decade has seen development of multiple

140 regional to continental flood models that span physically based approaches (e.g., 1-,2-, and 3-D

141 hydrodynamic models) to empirical models (including machine-learning approaches and statistical

142 models) (see review by Mudashiru et al. 2021). On the global scale, openly accessible global flood

143 models include those reviewed by Hoch and Trigg (2019), namely CaMa-Flood (Yamazaki et al. 2011),

144 GLOFRIS (Winsemius et al. 2013), JRC (Dottori et al. 2016), CIMA-UNEP (Rudari et al. 2015), Fathom

145 (Sampson et al. 2015), and ECMWF (Papperberger et al. 2012). For instance, Sampson et al. (2015)

146 created a global 90 m map of flood-prone areas between 60$^\circ$ N and 56$^\circ$ S using a regional flood-frequency

147 model. More recently, Nardi et al. (2019) developed published a global floodplain dataset at 250 m

148 resolution that extended from 60$^\circ$ N to 60$^\circ$ S, based developed through a on geomorphic or terrain-based

149 analyses of floodplain elevations and maximum flood-prone areas using on a drainage-area scaling

150 variable (Rajib et al. 2021). The evolution of the MERIT Hydro 90 m global hydrography dataset by

151 Yamazaki et al. (2019) and machine-learning approaches (e.g., Zhao et al. 2021) has created additional

152 opportunities to further advance the derivation of global floodplains, with improved identification of flow

153 accumulation area, river-basin shape, and river channel location.

154

155    These wetland-location and floodplain-extent data are critical for watershed-scale sustainable aquatic

156    resource policy decisions (Creed et al., 2017; Golden et al., 2017). The lack of these data can result in

157    disproportionately large model errors and potentially misguided management decisions when non-

158    floodplain wetlands are not incorporated in hydrological and biogeochemical models, ignoring their

159    watershed-scale impacts on flooding, drought, and water quality (Evenson et al., 2018a; Rajib et al., 2020;

160    Golden et al., 2021).

161

162    Here, we provide the first global geospatial dataset of non-floodplain wetlands. We incorporate the recent

163    development of a high-resolution global floodplain mapping algorithm based on digital terrain models by

164    Nardi et al. (2019). We couple these spatial floodplain data with higher-resolution modifications to the

165    gridded global wetland and open water data layers developed by Tootchi et al. (2019) that incorporate the

166    Pekel et al. (2016) satellite-based inundation product, modeled groundwater-driven wetland extent (Fan et

167    al. (2013), and ancillary satellite landcover data from Herold et al. (2015). We test the applicability of our

168    global dataset of non-floodplain wetlands in 21 large and spatial-data rich watersheds spanning nearly

169    700,000 km$^2$ across the CONUS. This novel global product identifying non-floodplain wetlands provides

170    for the quantification and estimation of the locations and extent of important aquatic systems with

171    abundant hydrological, biogeochemical, and biological functions, filling a noted research gap while

172    delivering useful data for informed natural resource decision-making and management (Creed et al.,

173    2017; Lane et al., 2022).

174

175    **2        Methodology and data**

176

177    Identifying global non-floodplain wetlands required the following steps: 1) determination of global

178    floodplain extent, 2) identification of the global distribution of wetlands, 3) spatial overlay (masking) of

179    floodplains and wetlands to derive a non-floodplain wetland data layer, and 4) data verification and

180    accuracy assessment. Steps 1-3 are outlined in a flow chart given in ~~Figure~~ Fig. 1.

181

## 2.1    Global floodplain data

183

Nardi et al. (2019) combined space-borne elevation data and terrain analysis with a novel open-source algorithm to delineate the geomorphic floodplains across the globe between 60°N and 60°S latitudes. Conceptually, Nardi et al. (2019) identified floodplains from surrounding hillslopes as those low-lying landscape features that have been naturally shaped by accumulated geomorphic effects of past flood events. The original Nardi et al. (2019) dataset was limited in its spatial extent (60°N-60°S) and resolution (250 m); this study sought to delineate global floodplain extent while concurrently identifying floodplain features further up the river network than possible with 250 m pixels. Hence, we utilized the freely available Nardi et al. (2019) GFPlain v1.0 algorithm and coupled this with the MERIT Hydro (Multi-Error Removed Improved Terrain, Yamazaki et al., 2019), global raster digital terrain model data to develop a higher resolution (90 m) geomorphic riverine floodplain for the globe, termed hereafter GFPlain90.

195

**Figure 1.** Data flow chart identifying the main data sets and processes involved in deriving the Global Floodplain

and Global Wetland data layers, as well as the intersection of those data to create the Global Non-floodplain

Wetlands data product. Curved boxes represent final products, and abbreviations may be found in the text and

Appendix A.

## 2.1 Global floodplain data

Nardi et al. (2019) combined space-borne elevation data and terrain analysis with a novel open-source algorithm to delineate the geomorphic floodplains across the globe between 60° N and 60° S latitudes. Conceptually, Nardi et al. (2019) identified floodplains from surrounding hillslopes as those low-lying landscape features that have been naturally shaped by accumulated geomorphic effects of past flood events. The original Nardi et al. (2019) dataset was limited in its spatial extent (60° N-60° S) and resolution (250 m); this study sought to delineate global floodplain extent while concurrently identifying floodplain features further up the river network than possible with 250 m pixels. Hence, we utilized the freely available Nardi et al. (2019) GFPlain v1.0 algorithm and coupled this with the MERIT Hydro (Multi-Error Removed Improved Terrain, Yamazaki et al., 2019), global raster digital terrain model data to develop a higher resolution (90 m) geomorphic riverine floodplain for the globe, termed hereafter GFPlain90.

The development of GFPlain90 required multiple steps. We first extracted elevation data from MERIT Hydro and, reprojected the data in UTM zones to prevent distortion when using the GFPlain algorithm. We then and then developed the drainage network, drainage area, flow accumulation and flow direction data from these data using the established scaling parameters in Nardi et al. (2019; power-law coefficient ($a$) of 0.01 and dimensionless exponent ($b$) = 0.30)). We established 20 km$^2$ as the minimum contributing-area threshold required to create the drainage network, balancing the development of a global stream-network distribution and extent with computational requirements. We then globally organized the data by HydroBASINS Level 4 basins (Lehner and Grill, 2013). HydroBASINS provides seamless watershed boundaries and subbasin delineations at global scales; there are 1,342 Level 4 HydroBASINS globally. The floodplain extent resolution of GFPlain90 was resampled (using nearest neighbor) to 30 m for subsequent performance assessment and overlap analyses with the wetland spatial data. All spatial

225    analyses in this study were conducted using ArcGIS Pro v.2.9.x (ESRI, Redlands, California) and GRASS

226    GIS v 7.4.4 (OSGEO, Beaverton, Oregon).

227

228    **2.2      Global Wetland data**

229

230    Tootchi et al. (2019) developed a widely used composite global wetland map at ~500 m by combining

231    multiple data sources, including both satellite-based surface-water inundation mapping and vegetation

232    classification coupled with model-based approaches capturing important groundwater-driven wetland

233    systems. We specifically used the Tootchi et al. (2019) composite map consisting of both regularly

234    surface-water flooded wetlands ("regularly flooded wetlands," RFWs) and groundwater discharge-

235    maintained wetlands ("groundwater-driven wetlands," GDWs) as the foundation for our global wetland

236    map. Tootchi et al. (2019) merged the RFW and GDW maps, described below, to form a union product

237    used here that demonstrated a high correlation with available evaluation data, called the composite

238    wetland-water table depth (or CW-WTD).

239

240    **2.2.1    Original composite wetland data**

241

242    Regularly flooded wetlands (RFWs) derived by Tootchi et al. (2019) were based on three data sources: 30

243    m resolution Global Surface Water (GSW) by Pekel et al. (2016), 300 m Climate Change Initiative (CCI)

244    land cover data by Herold et al. (2015), and 500 m GIEMS-D15 wetland extent data by Fluet-Chouinard

245    et al. (2015). GSW data used by Tootchi et al. (2019) were developed from Landsat satellite imagery

246    analyses of pixels identified as inundated at least once during the 32-year period of record by Pekel et al.

247    (2016). CCI input wetland data for Tootchi et al. (2019) included both inundated and wetland vegetation-

248    classed pixels assessed during the period 2008-2012 by Herold et al. (2015). For GIEMS-D15, data

249    included were the mean annual maximum extent of pixels identified as wetlands using multi-sensor

250    satellite data by Prigent et al. (2007), downscaled to ~500 m resolution by Fluet-Chouinard et al. (2015).

251 GSW and CCI input data were resampled to ~500 m resolution using an "all or nothing" approach by

252 Tootchi et al. (2019). This means that a pixel categorization of "wetland" at 500 m resolution was given

253 by Tootchi et al. (2019) only if the majority of resampled finer-resolution input pixels were classed as

254 wetlands. The upward resampling from 30 m and 300 m to 500 m resulted in a loss of informative spatial

255 data on wetland extent from GSW and CCI. Tootchi et al. (2019) calculated that RFWs cover

256 approximately 9.7 % of the global land area (excluding lakes [sourced from (Messager et al., 2016)],

257 Antarctica, and the Greenland ice sheet).

258

259 Groundwater-driven wetlands (GDWs in the analysis of Tootchi et al., 2019) used in this study were

260 based on the water-table depth estimates by Fan et al. (2013). Fan et al. (2013) developed a 1 km

261 resolution groundwater map based on climate and terrain variables that was validated by over 1 million

262 government-recorded and published observations. Fan et al. (2013) estimated that shallow groundwater

263 influenced nearly 15 % of groundwater-fed surface features, explaining important wetland patterning at

264 global scales (as well as vegetation classes at local and regional scales). A water-table depth threshold of

265 ≤ 20 cm was used by Tootchi et al. (2019) to identify groundwater-driven wetlands and they resampled

266 these data to ~500 m cell resolution. The GDW distribution based on water table depths covered

267 approximately 15 % of the global land mass (including large portions of the Amazon basin, coastal zones,

268 and North American and Siberian peatlands).

269

270 Tootchi et al. (2019) created a merged "final" product, which that called the composite wetland-water

271 table depth (CW-WTD) map, which is based on the union of the merged the RFW and GDW maps to

272 form a union product with a high correlation with available evaluation data, which they called the

273 composite wetland-water table depth (hereafter CW-WTD). They measured an approximately 3.8 %

274 overlap between the total land pixels identified as wetlands in both the RFW and GDW maps that

275 comprise the CW-WTD, suggesting the different input maps capture different wetland types. At the

276    global scale, Tootchi et al. (2019) reported spatial Pearson correlations between CW-WTD (wetland

277    fractions at 3 arcmin, or ~4.9 km grids) and wetlands within GLWD (Lehner and Döll, 2004) and Hu et

278    al. (2017b) as r=0.34 and r=0.43, respectively. Tootchi et al. (2019, their Table 5 and S1) provided

279    additional analysis of the correlations between their global wetland product and existing benchmark data.

280    The total CW-WTD global wetland estimate was ~ 21.1 % of the land mass, or approximately 27.5

281    million km$^2$ (excluding large lakes, Antarctica, and the Greenland ice sheet; Tootchi et al., 2019).

282

283    **2.2.2    Derived global wetland data**

284

285    To account for the acknowledged limitations of the Tootchi et al. (2019) data and to accurately identify

286    more of the existing small and, specifically, non-floodplain wetlands across the globe (e.g., those <25 ha),

287    we improved upon and augmented the CW-WTD (Tootchi et al., 2019) global wetland data layer with the

288    30 m native-resolution GSW (Pekel et al., 2016) and 300 m native-resolution CCI (Herold et al., 2015)

289    data. The inclusive wetland categories of Tootchi et al. (2019) were maintained, namely at least one

290    inundation event over a 32 year range (for GSW data) and CCI pixels defined as "…mixed classes of

291    flooded areas with tree covers, shrubs, or herbaceous covers plus inland water bodies…" (Tootchi et al.,

292    2019, p. 193). However, for our analysis we resampled the 500 m CW-WTD product to 30 m using the

293    nearest-neighbor approach and then added any identified wetland pixel from the CCI data (resampled

294    from 300 m to 30 m) and inundated pixel from the GSW data (30 m resolution). Resampling to a finer

295    resolution (as we did in our analysis ) does not result in data losses : the same data are retained but are

296    divided into equal, smaller parts. ~~However, moving from a finer resolution to coarser resolution causes~~

297    ~~data losses: fine-scale data are necessarily aggregated (often by averaging) to a larger grid cell size, and~~

298    ~~therefore less information is retained.~~ However, moving from a finer resolution to coarser resolution (as

299    in the CW-WTD dataset's "all-or-nothing" approach) does cause data losses: fine-scale data are

300    necessarily aggregated (often by averaging) to a larger grid cell size, and therefore less information is

301    retained. To compensate for this data loss in the CW-WTD dataset, the finer resolution ~~JRC~~GSW ~~data~~ (30

302 m) and CCI (300 m) data ~~was~~were added back into the dataset. ~~Resampling to a finer resolution does not~~

303 ~~result in a loss of any data whereas resampling from a finer resolution to a coarser resolution results in the~~

304 ~~loss of any data smaller than the chosen resolution.~~ This resulted in a novel and encompassing wetland

305 ensemble end-product, hereafter termed the Global Wetlands dataset. This new dataset is inclusive of both

306 finer-resolution (30 m and 300 m) data, thereby accounting for a wide range of wetland sizes – such as

307 smaller non-floodplain wetlands (Cohen et al., 2016) – that remained unmapped by Tootchi et al. (2019).

308

309 **2.3     Global Non-Floodplain Wetlands (Global NFWs)**

310

311 To identify non-floodplain wetlands specifically, we overlaid our GFPlain90 floodplain data with our

312 mapped Global Wetlands data to mask wetland pixels collocated on the floodplain. Then, to avoid tidally

313 influenced wetlands, we conducted a region-group analysis to identify connected pixels abutting coastal

314 shorelines in order to mask wetlands in coastal areas (e.g., those directly abutting the shoreline and

315 spatially connected to tidally influenced areas). We used a four-directional contagion criterion to identify

316 connected pixels (i.e., those connected in cardinal directions). Subsequently, we applied a 1 km buffer to

317 the HydroBASINS (Lehner and Grill, 2013) coastline area and removed from our analyses any wetland

318 region-group partially or completely overlain by the 1 km coastline buffer. In addition, Tootchi et al.

319 (2019) removed lake systems ($\geq$ 10 ha) from their wetland-focused data by masking aquatic layers using

320 HydroLAKES (Messager et al., 2016). To avoid including large lakes in our emerging non-floodplain

321 wetland geospatial data, we also applied the HydroLAKES mask and removed lake systems $\geq$ 10 ha

322 (Messager et al., 2016) from our Global Wetlands dataset. Thus, our final global non-floodplain wetland

323 data product (hereafter Global NFWs) did not include fluvial floodplain wetlands nor coastal wetland

324 complexes and large open water lacustrine (lake-like, Cowardin et al., 1979) systems.

325

326 **2.4     Data verification and assessment**

327

328      We evaluated the global products developed here through comparison of high-resolution floodplain and

329      wetland extent data from 21 basins representing disparate climatic (according to the Köppen-Geiger

330      classification, Beck et al., 2018), elevation, and land-use gradients within the CONUS (Fig. 2;

331      summarized in Table B1B2). We specifically focused on the CONUS for product assessment because of

332      its wide-ranging data availability and diversity of physiographic and climatic regions.

333

334      **2.4.1     Verifying floodplain extent**

335

336      We used a recently developed machine learning (ML)-based 30 m resolution CONUS floodplain dataset

337      (Woznicki et al., 2019) as the benchmark to evaluate our GFPlain90 global floodplain data. Specifically,

338      the ML model by Woznicki et al. (2019) used the U.S. Federal Emergency Management Agency (FEMA)

339      100 yr floodplain (i.e., a 1 % chance of coastal or fluvial flood-inundation in a given year; Jakubínský et

340      al., 2021) as the training data, and subsequently used soil and topographic characteristic along with land

341      cover to identify potential floodplain grid cells across CONUS at 30 m resolution. Woznicki et al. (2019)

342      reported that their ML approach correctly identified ~79 % of the FEMA 100 yr coastal and fluvial

343      floodplains, providing spatially complete 100 yr floodplain coverage totaling 980,450 $km^2$ across the

344      CONUS.

345

346      **2.4.2     Verifying wetland and non-floodplain wetland extent**

347

348      We evaluated our inclusive Global Wetlands and Global NFWs datasets in 21 basins covering ~680,000

349      $km^2$ (Fig. 2). We contrasted our products to the 2016 National Land Cover Database (NLCD, Dewitz,

350      2019). The NLCD is a 30 m Landsat satellite-based geospatial product with an overall accuracy of 86 %

351      that incorporates high-resolution aerial imagery of wetland location for model parameterization and

352      calibration (Jin et al., 2019; Wickham et al., 2021). Three NLCD classes were selected for comparison

353      with the Global Wetland product: woody wetlands, emergent herbaceous wetlands, and open water. To

354

355
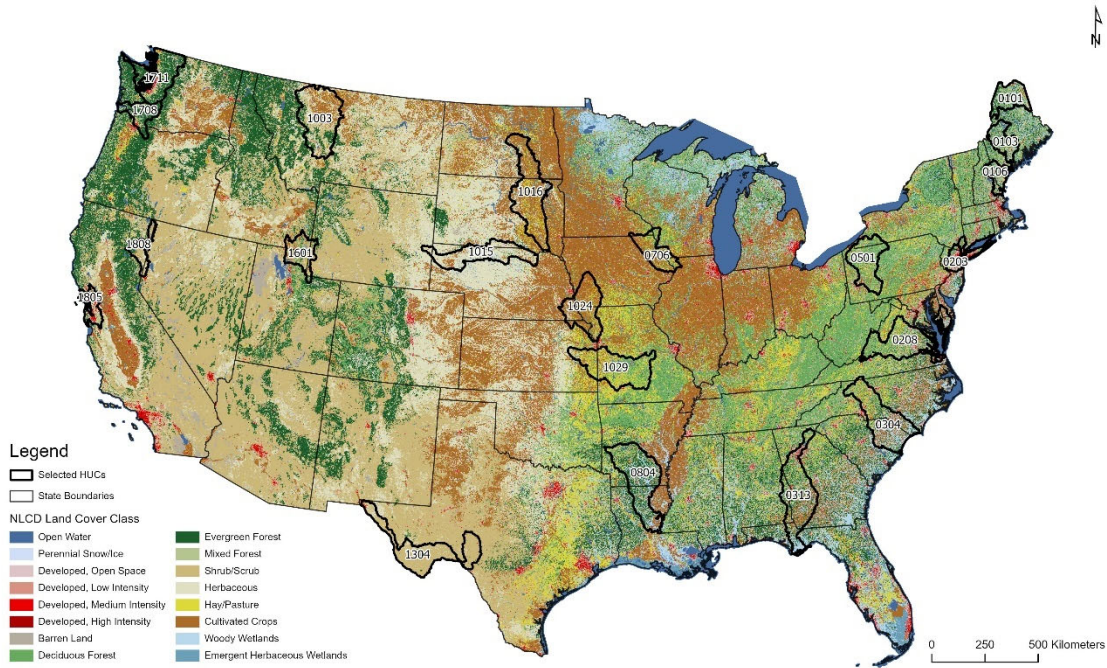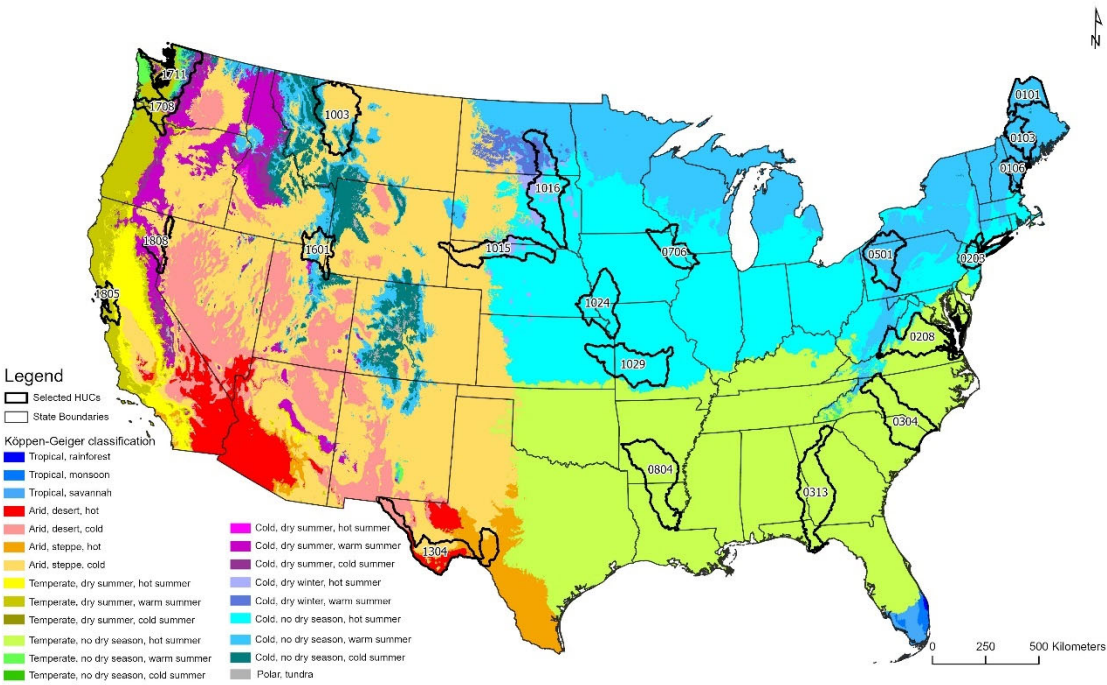
**Figure 2.** Twenty-one validation watersheds were selected from across CONUS to capture the breadth and extent of land use (top, NLCD 2019) and climate and physiographic regions (bottom) within CONUS according to the Köppen-Geiger classification (Beck et al., 2018); also summarized in Table B1B2). Land cover data are from NLCD (2019) and tThe Hydrologic Unit Code (HUC) classifications are sourced from USGS Watershed Boundary Dataset (2022).

361

assess the relative improvement of our 30 m Global Wetlands and Global NFWs dataset with the 500 m

Tootchi et al. (2019) data, we also contrasted the CW-WTD with the NLCD classes within the

verification watersheds. For equal comparisons, following Tootchi et al. (2019) we used the Messager et

al. (2016) HydroLAKES to mask out large lake systems ($\geq$ 10 ha) from both the Global Wetlands and the

NLCD data within the 21 verification watersheds.

### 2.4.3    Standard performance measures

We evaluated the floodplain and wetland spatial data within the 21 validation watersheds using

commonly employed performance measures. Following Wing et al. (2017), we first created a contingency

table for our performance assessment (Table 1). As noted, we selected 20 km$^2$ as the minimum

contributing area to develop stream networks in our global floodplain analysis, a reasonable area for flow-

accumulation that balances computational efficiency for global geospatial model development. Woznicki

et al. (2019), our benchmark floodplain dataset, used a 4.5 km$^2$ contributing area in their high-resolution

CONUS analysis. To appropriately compare between datasets of two varying resolutions, we removed

stream and river network components from the Woznicki et al. (2019) validation dataset developed with

contributing areas <20 km$^2$, as our model did not discern landscape data at that granularity.

**Table 1.** Contingency table of possible outcomes for each cell used in assessing the performance of either the

floodplain or wetland geospatially modeled data. We contrasted published benchmark data from Woznicki et al.

(2019) for floodplain extent against modeled GFPlain90 data. Wetland comparisons contrasted NLCD wetlands

(Dewitz, 2019, open water and wetland classes) against both Global Wetlands and Global NFWs data. Table is

modified from Wing et al. (2017). The subscript "1" equates to a positive outcome or overlapping extent for either

the modeled (M) or benchmark (B) data whereas a zero means no data overlap or a negative outcome.

|  | Floodplain [or Wetland]<br>in Benchmark data | Not Floodplain [or Wetland]<br>in Benchmark data |
|---|---|---|

| | | |
|---|---|---|
| **Floodplain [or Wetland] in Modeled data** | $M_1B_1$ | $M_1B_0$ |
| **Not Floodplain [or Wetland] in Modeled data** | $M_0B_1$ | $M_0B_0$ |

386

387 CONUS analysis. To appropriately compare between datasets of two varying resolutions, we removed

388 stream and river network components from the Woznicki et al. (2019) validation dataset developed with

389 contributing areas <20 $km^2$, as our model did not discern landscape data at that granularity.

390

391 To provide a full assessment of our geospatial modeling performance, we contrasted our GFPlain90

392 floodplain dataset across the 21 validation watersheds using the approaches described below following

393 Sampson et al. (2015), Wing et al. (2017), and others (e.g., Bates and De Roo, 2000; Alfieri et al., 2014;

394 Sangwan and Merwade, 2015; Jafarzadegan et al., 2018; Woznicki et al., 2019). We first contrasted our

395 GFPlain90 floodplains to Woznicki et al. (2019), our benchmark floodplain data. We then analyzed the

396 watershed-scale comparison of our Global Wetlands product versus the NLCD wetlands (combined open

397 water and wetland classes), our benchmark wetlands data. We followed with a comparison focusing only

398 on our Global NFWs data and those NLCD wetlands and open water pixels that were determined to be

399 non-floodplain systems (i.e., NLCD data that also do not overlap the GFPlain90 data nor coastal waters

400 and with lakes >10 ha removed). These NLCD wetlands were our benchmark non-floodplain wetland

401 data. Lastly, we assessed the mean and aggregate error bias of our analyses by exploring results at coarser

402 spatial granularity (i.e., 1 km pixel size) along the riverine network (for floodplain assessment) and, for

403 wetland metrics, throughout the entirety of our 21 performance assessment watersheds (Sampson et al.,

404 2015; Wing et al., 2017). The metrics described below and in Table 2 were used in our analyses.

405

406

407 *Hit Rate* (Bates and De Roo, 2000; Horritt and Bates, 2002; Tayefi et al., 2007) also referred to as Recall

408 (Woznicki et al., 2019) and Correct (Sangwan and Merwade, 2015), measures how well a geospatial

409 model classification replicates the benchmark data but does not penalize for overprediction. *H* varies from

410 0, where there is no overlap between the modeled data and the benchmark data, to 1 where the modeled

411 data completely contain the benchmark data. *Precision* (Woznicki et al., 2019), also known as Spatial

412 Coincidence (Tootchi et al., 2019), indicates the proportion of the benchmark data that are correctly

413 predicted and mapped in the modeled data. This metric, *P*, also ranges from 0 to 1 with higher values

414 **Table 2.** Performance metrics used in validation assessments of floodplain and wetland data layers. Data for

415 assessment (e.g., $M_1B_1$) follow that given in Table 1 and modified from Wing et al. (2017), with the exception of

416 equations 7 and 8 (see text).

| Equation Number | Metrics | Equation | Range |
|---|---|---|---|
| 1 | **Hit Rate (H)** | $Hit\ Rate\ (H) = \frac{M_1B_1}{M_1B_1 + M_0B_1}$ | 0 - 1, higher is "better" |
| 2 | **Precision (P)** | $Precision\ (P) = \frac{M_1B_1}{M_1B_1 + M_1B_0}$ | 0 - 1, higher is "better" |
| 3 | **False Alarm Ratio (FA)** | $False\ Alarm\ Ratio\ (FA) = \frac{M_1B_0}{M_1B_0 + M_1B_1}$ | 0 - 1, lower is "better" |
| 4 | **Critical Success Index (CSI)** | $Critical\ Success\ Index\ (CSI) = \frac{M_1B_1}{M_1B_1 + M_0B_1 + M_1B_0}$ | 0 - 1, higher is "better" |
| 5 | **F1** | $F1 = 2\left(\frac{H \times P}{H + P}\right)$ | 0 - 1, higher is "better" |
| 6 | **Error Bias (EB)** | $Error\ Bias\ (EB) = \frac{M_1B_0}{M_0B_1}$ | 0 - ∞; <1 underprediction, 1 = no bias, >1 indicate overprediction |
| 7 | **Mean Absolute Error ($E_A$)** | $Mean\ Absolute\ Error\ (E_A) = \frac{\sum_{i=1}^{N}|M-B|}{N}$ | 0 - 1, lower is "better" |
| 8 | **Aggregate Error Bias ($B_A$)** | $Aggregate\ Error\ Bias\ (B_A) = \frac{\sum_{i=1}^{N}M-B}{N}$ | -1 to 1, negative values indicate underprediction, positive values overprediction |

417

418 —indicating better performance. The *False Alarm Ratio* ( Sampson et al., 2015; Wing et al., 2017) also

419 known as the False Discovery Ratio, quantifies modeled data overprediction relative to the benchmark

420 ~~*Hit Rate* (Bates and De Roo, 2000; Horritt and Bates, 2002; Tayefi et al., 2007; Alfieri et al., 2014;~~

421 ~~Sampson et al., 2015; Wing et al., 2017; Jafarzadegan et al., 2018) also referred to as Recall (Woznicki et~~

422 ~~al., 2019) and Correct (Sangwan and Merwade, 2015), measures how well a geospatial model~~

423 ~~classification replicates the benchmark data but does not penalize for overprediction. *H* varies from 0,~~

424 ~~where there is no overlap between the modeled data and the benchmark data, to 1 where the modeled data~~

425 ~~completely contain the benchmark data.~~

$$Hit\ Rate\ (H) = \frac{M_1 B_1}{M_1 B_1 + M_0 B_1} \qquad (1)$$

427

428 *~~Precision~~* ~~(Woznicki et al., 2019), also known as Spatial Coincidence (Tootchi et al., 2019), indicates the~~

429 ~~proportion of the benchmark data that are correctly predicted and mapped in the modeled data. This~~

430 ~~metric, *P*, also ranges from 0 to 1 with higher values indicating better performance.~~

$$Precision\ (P) = \frac{M_1 B_1}{M_1 B_1 + M_1 B_0} \qquad (2)$$

432

433 ~~The *False Alarm Ratio* ( Sampson et al., 2015; Wing et al., 2017) also known as the False Discovery~~

434 ~~Ratio, quantifies modeled data overprediction relative to the benchmark~~ data. *F* varies from 0 (zero false

435 alarms) to 1 (all false alarms); lower values are considered better performance. The False Alarm Ratio can

436 also be calculated as 1 - *Precision* (Woznicki et al., 2019).

$$False\ Alarm\ Ratio\ (FA) = \frac{M_1 B_0}{M_1 B_0 + M_1 B_1} \qquad (3)$$

438

439 The *Critical Success Index* (CSI,  Bates and De Roo, 2000; Aronica et al., 2002; Werner et al., 2005;

440 Fewtrell et al., 2008~~; Alfieri et al., 2014; Sampson et al., 2015; Wing et al., 2017~~), also known as

441 Jaccard's Index (Tootchi et al., 2019), and Fit (Sangwan and Merwade, 2015), penalizes for both over-

442 and under-prediction, ranging from 0 (no match) to 1 (perfect match).

$$Critical\ Success\ Index\ (CSI) = \frac{M_1 B_1}{M_1 B_1 + M_0 B_1 + M_1 B_0} \qquad (4)$$

444

445 Woznicki et al. (2019) utilized a performance metric, *F1*, which combines the *Hit Rate* (called Recall by

446 Woznicki et al. 2019) and *Precision* using their harmonic mean. *F1* also varies from 0 to 1, with higher

447 values indicating better performance.

$$F1 = 2\left(\frac{H \times P}{H + P}\right) \qquad (5)$$

449

450  *Error Bias* (*EB*) characterizes the tendency of the model towards under- or over-prediction (Sampson et

451  al., 2015). Values of 1 indicate no bias, $0 \leq EB < 1$ indicates underprediction whereas $1 < EB \leq \infty$

452  indicates the model is tending towards overprediction.

453  $$\textit{Error Bias (EB)} = \frac{M_1 B_0}{M_0 B_1} \qquad \text{(6)}$$

454

455  Lastly, two additional metrics were calculated that assessed performance at the 30 arc-sec (~1 km) scale.

456  These measures, *Mean Absolute Error* and *Aggregate Error Bias* (Sampson et al., 2015; Wing et al.,

457  2017), characterize the data accuracy across large spatial extents. Large spatial extents are areas where 30

458  m data and overlap accuracy is less a concern than general dataset performance for broad-scale end-user

459  applications (e.g., when coarser, watershed-scale "lumped" hydrologic characterizations of water storage

460  are all that is required). For these metrics, both estimated and benchmark data were resampled to 1 km

461  resolution across the whole of each watershed; values within each 1 km pixel ranged from 0 to 1 and

462  represented the fraction of the 30 m resolution estimates and benchmark data. We assessed floodplain

463  estimates after calculating the fractional abundance comprising each 1 km$^2$ pixel within a 1 km buffer

464  around the Woznicki et al. (2019) floodplain data. We additionally analyzed all wetlands at the

465  watershed-scale as well as focusing on non-floodplain wetlands (e.g., wetlands exclusive of the

466  GFPlain90 floodplain or coastal connections, our target aquatic system). In Eq. 7 and 8 (given in Table 2),

467  $$\text{(7)} \qquad \textit{Mean Absolute Error (E\textsubscript{A})} = \frac{\sum_{i=1}^{N} |M - B|}{N}$$

468

469  $$\textit{Aggregate Error Bias (B\textsubscript{A})} = \frac{\sum_{i=1}^{N} M - B}{N} \qquad \text{(8)}$$

470

471  ~~Where~~ *M* is the area estimated as floodplain (or wetland), *B* is the benchmark floodplain (or wetland)

472  area, and *N* is the number of 1 km cells with data. *Mean Absolute Error* and *Aggregate Error Bias* were

473  calculated for each of the 21 HUCs, following Wing et al. (2017).

474

475

476  **3      Results**

477

478  **3.1     Floodplain data performance**

479

480  The GFPlain90 floodplain data (Fig. 3) performed well when contrasted with the 100 yr coastal and

481  fluvial floodplain extent data from Woznicki et al. (2019), even though our analyses do not map coastal

482  floodplains. A median Hit Rate of 0.77 suggests that nearly 80% of the benchmark floodplain from

483  Woznicki et al. (2019) was similarly captured by the GFPlain90 floodplain data (see Appendix Table

484  2B3). In addition, the median False Alarm of 0.26 indicates that for every three pixels correctly identified

485  as within the Woznicki et al. (2019) floodplain, one pixel was incorrectly identified as such (i.e., a

486  commission error measure); this is evident in wider GFPlain90 floodplains in lower river reaches than

487  predicted by Woznicki et al. (2019). These performance values are similar to those reported by Woznicki

488  et al. (2019, False Alarm 0.22) and Wing et al. (2017, False Alarm 0.34-0.37). Critical Success Index

489  (CSI) scores penalize for over-prediction; our median value of 0.53 approximates previously published

490  regional (e.g., Sangwan and Merwade, 2015, CSI values ranging from 0.44-0.89) and continental flood-

491  extent approaches (e.g., Sampson et al., 2015, CSI values from 0.43-0.67; Wing et al., 2017; CSI values

492  between 0.50 and 0.55 reported). Median Precision (0.74) and F1 (0.70) values approximate those in the

493  literature as well (e.g., Woznicki et al., 2017 reported values of 0.78 for both). Median Error Bias values

494  of 1.0 suggests the model neither over-estimates nor under-estimates floodplain extents (Wing et al.

495  2017). Mean Absolute Error of 0.08 reported here indicates an approximate 8 % difference between our

496  GFPlain90 model and that of Woznicki et al. (2017) at the 1 km cell resolution.

497

498  **3.2      Wetland data performance**

499

500  **3.2.1    Global Wetland dataset**

501

502 The novel ensemble Global Wetlands approach improved upon the previously published Tootchi et al.

503 (2019) research product, the CW-WTD (Table 3) when contrasted with CONUS data. A median Hit Rate

504 value of 0.24 indicates that both the inclusive Global Wetlands and CW-WTD captured ~one-quarter of

505 the high-resolution, 30-m pixel size NLCD wetlands and open waters in the validation dataset. However,

506 across the 21 validation watersheds the Global Wetlands dataset developed here correctly identified more

507 wetlands than the CW-WTD alone, as indicated by an 8% mean increase in Precision, 43 % increase in

508 Critical Success Index, 38 % increase in F1, a -8 % decrease in the False Alarm ratio, and a 21 %

509 decrease in Error Bias. At coarser, 1 km$^2$ scales, there was a slight decrease in the Mean Absolute Error

510 associated with the Global Wetlands, and no difference in Aggregate Error Bias between the data

511 products.

512

513

**Figure 3.** The robust performance of GFPlain90 relative to the benchmark Woznicki et al. (2019) floodplain data is

evident in the two rows, with the top panels (HUC_0304) a coastal watershed spanning North and South Carolina,

USA, and the bottom two panels different spatial extents of a midwestern USA watershed (HUC_1024). The

mainstem of the river network appeared wider in the GFPlain90 data in both examples, especially in the lower

reaches, though the complete network was well represented (i.e., floodplains were identified to the furthest extent of

the stream network's headwaters). Satellite imagery is are sourced from ESRI (2022).

decrease in Error Bias. At coarser, 1 km$^2$ scales, there was a slight decrease in the Mean Absolute Error associated with the Global Wetlands, and no difference in Aggregate Error Bias between the data products. **Table 2.** Floodplain performance assessment of the GFPlain90-derived floodplain and the benchmark floodplain from Woznicki et al. (2019). The first six equations directly assess the spatial concordance and overlap between the two datasets, whereas Mean Absolute Error (Eq. 7) and Aggregate Error Bias (Eq. 8) are coarser fractional analyses (i.e., the fraction of a 1 km$^2$ cell predicted correctly) as measured along the riverine network.

### 3.2 Wetland data performance

#### 3.2.1 Global Wetland dataset

The novel ensemble Global Wetlands approach improved upon the previously published Tootchi et al. (2019) research product, the CW-WTD (Table 3) when contrasted with CONUS data. A median Hit Rate value of 0.24 indicates that both the inclusive Global Wetlands and CW-WTD captured ~one-quarter of the high-resolution, 30-m pixel size NLCD wetlands and open waters in the validation dataset. However, across the 21 validation watersheds the Global Wetlands dataset developed here correctly identified more wetlands than the CW-WTD alone, as indicated by an 8% mean increase in Precision, 43 % increase in Critical Success Index, 38 % increase in F1, a -8 % decrease in the False Alarm ratio, and a 21 % decrease in Error Bias. At coarser, 1 km$^2$ scales, there was a slight decrease in the Mean Absolute Error associated with the Global Wetlands, and no difference in Aggregate Error Bias between the data products.

### 3.2.2 Global Non-Floodplain Wetland (Global NFW) dataset

546    Non-floodplain wetland identification using the Global Wetlands data (i.e., Global NFWs) similarly

547    improved upon the CW-WTD product (Fig. 4). For instance, though the Hit Rate values were low (e.g.,

548    median values ≤ 0.10), underscoring both the difficulty in mapping non-floodplain wetlands and the

549    challenge of assessing performance using high-resolution data, Global NFW analyses correctly identified

550    50 % more non-floodplain wetlands than the CW-WTD (Table 4, Tootchi et al., 2019). Improvements

551    when focusing on non-floodplain wetlands were found in every category with the Global NFWs dataset,

552    demonstrating increased non-floodplain wetland accuracy versus the original CW-WTD across the

553    median metric values for Precision, Critical Success Index, F1, False Alarms, and Error Bias (e.g., 33 %

554    increase in Precision, 20 % increase in Critical Success Index, 10 % increase in F1 scores, and a 12 %

555    decrease in False Alarms and a 19 % decrease in Error Bias). There was no difference between the

556    datasets with median values for Mean Absolute Error (median values for both = 0.09) or Aggregate Error

557    Bias (median values for both = 0.07). Thus, at the 1 km$^2$ cell size, there was <10 % difference between

558    both the CW-WTD and the Global NFWs and the benchmark NLCD non-floodplain wetlands and open

559    waters (with the difference mostly stemming from an increase in identified wetlands with both CW-WTD

560    and Global NFWs, as indicated with the positive Aggregate Error Bias values).

561

562

563

564

**Table 3.** Spatial performance assessment of both the Global Wetland (abbreviated here as GW) and CW-WTD

(abbreviated here as WTD, Tootchi et al., 2019) datasets when contrasted with the benchmark NLCD wetlands

(Dewitz, 2019). The first six equations directly assess the spatial concordance and overlap between each spatial

dataset and the benchmark (e.g., CW-WTD contrasted with the NLCD), whereas Mean Absolute Error (MAE, Eq.

7) and Aggregate Error Bias (AEB, Eq. 8) are coarser fractional analyses measured throughout each watershed (e.g.,

the proportional abundance NLCD within each 1 km$^2$ cell is contrasted with the proportional abundance of Global

Wetlands predicted correctly within that cell).

| Hydrologic Unit Code (HUC) ID | Hit Rate (Eq. 1) | | Precision (Eq. 2) | | False Alarm (Eq. 3) | | Critical Success (Eq. 4) | |
|---|---|---|---|---|---|---|---|---|
| | WTD | GW | WTD | GW | WTD | GW | WTD | GW |
| HUC_0101 | 0.31 | 0.32 | 0.51 | 0.53 | 0.49 | 0.47 | 0.24 | 0.25 |
| HUC_0103 | 0.26 | 0.28 | 0.42 | 0.45 | 0.58 | 0.55 | 0.19 | 0.21 |
| HUC_0106 | 0.25 | 0.27 | 0.41 | 0.44 | 0.59 | 0.56 | 0.18 | 0.20 |
| HUC_0203 | 0.12 | 0.12 | 0.51 | 0.53 | 0.49 | 0.47 | 0.11 | 0.11 |
| HUC_0208 | 0.31 | 0.33 | 0.56 | 0.65 | 0.44 | 0.35 | 0.25 | 0.28 |
| HUC_0304 | 0.42 | 0.43 | 0.65 | 0.69 | 0.35 | 0.31 | 0.35 | 0.36 |
| HUC_0313 | 0.39 | 0.41 | 0.58 | 0.64 | 0.42 | 0.36 | 0.30 | 0.33 |
| HUC_0501 | 0.15 | 0.17 | 0.57 | 0.64 | 0.43 | 0.36 | 0.14 | 0.15 |
| HUC_0706 | 0.24 | 0.25 | 0.86 | 0.92 | 0.14 | 0.08 | 0.23 | 0.24 |
| HUC_0804 | 0.45 | 0.46 | 0.70 | 0.75 | 0.30 | 0.25 | 0.38 | 0.40 |
| HUC_1003 | 0.14 | 0.16 | 0.32 | 0.41 | 0.68 | 0.59 | 0.11 | 0.13 |
| HUC_1015 | 0.25 | 0.40 | 0.17 | 0.42 | 0.83 | 0.58 | 0.12 | 0.26 |
| HUC_1016 | 0.13 | 0.16 | 0.54 | 0.70 | 0.46 | 0.30 | 0.12 | 0.15 |
| HUC_1024 | 0.10 | 0.10 | 0.67 | 0.75 | 0.33 | 0.25 | 0.09 | 0.10 |
| HUC_1029 | 0.10 | 0.13 | 0.51 | 0.72 | 0.49 | 0.28 | 0.09 | 0.13 |
| HUC_1304 | 0.02 | 0.02 | 0.44 | 0.52 | 0.56 | 0.48 | 0.02 | 0.02 |
| HUC_1601 | 0.29 | 0.33 | 0.34 | 0.45 | 0.66 | 0.55 | 0.19 | 0.24 |
| HUC_1708 | 0.24 | 0.24 | 0.48 | 0.49 | 0.52 | 0.51 | 0.19 | 0.20 |
| HUC_1711 | 0.09 | 0.10 | 0.46 | 0.51 | 0.54 | 0.49 | 0.08 | 0.09 |
| HUC_1805 | 0.14 | 0.15 | 0.62 | 0.64 | 0.38 | 0.36 | 0.13 | 0.13 |
| HUC_1808 | 0.12 | 0.13 | 0.51 | 0.55 | 0.49 | 0.45 | 0.11 | 0.11 |
| Median | 0.24 | 0.24 | 0.51 | 0.55 | 0.49 | 0.45 | 0.14 | 0.20 |
| Difference | | 0.00 | | 0.04 | | -0.04 | | 0.06 |
| Change (%) | | 0.0 | | 7.8 | | -8.2 | | 42.9 |

     **Table 3.** (Continued)

| Hydrologic Unit Code (HUC) ID | F1 (Eq. 5) | | Error Bias (Eq. 6) | | MAE (Eq. 7) | | AEB (Eq. 8) | |
|---|---|---|---|---|---|---|---|---|
| | WTD | GW | WTD | GW | WTD | GW | WTD | GW |
| **HUC_0101** | 0.38 | 0.40 | 0.43 | 0.40 | 0.18 | 0.17 | 0.09 | 0.09 |
| **HUC_0103** | 0.32 | 0.34 | 0.50 | 0.47 | 0.16 | 0.15 | 0.06 | 0.07 |
| **HUC_0106** | 0.31 | 0.33 | 0.49 | 0.46 | 0.20 | 0.19 | 0.08 | 0.08 |
| **HUC_0203** | 0.19 | 0.20 | 0.13 | 0.13 | 0.36 | 0.36 | 0.28 | 0.28 |
| **HUC_0208** | 0.40 | 0.44 | 0.35 | 0.27 | 0.17 | 0.17 | 0.09 | 0.10 |
| **HUC_0304** | 0.51 | 0.53 | 0.39 | 0.34 | 0.21 | 0.21 | 0.12 | 0.13 |
| **HUC_0313** | 0.47 | 0.50 | 0.48 | 0.38 | 0.16 | 0.16 | 0.07 | 0.09 |
| **HUC_0501** | 0.24 | 0.26 | 0.14 | 0.11 | 0.10 | 0.10 | 0.09 | 0.09 |
| **HUC_0706** | 0.37 | 0.39 | 0.05 | 0.03 | 0.12 | 0.12 | 0.11 | 0.12 |
| **HUC_0804** | 0.55 | 0.57 | 0.36 | 0.29 | 0.20 | 0.20 | 0.12 | 0.14 |
| **HUC_1003** | 0.19 | 0.23 | 0.34 | 0.27 | 0.04 | 0.04 | 0.02 | 0.02 |
| **HUC_1015** | 0.21 | 0.41 | 1.59 | 0.91 | 0.05 | 0.04 | -0.01 | 0.00 |
| **HUC_1016** | 0.21 | 0.26 | 0.13 | 0.08 | 0.26 | 0.26 | 0.23 | 0.24 |
| **HUC_1024** | 0.17 | 0.18 | 0.05 | 0.04 | 0.14 | 0.14 | 0.13 | 0.14 |
| **HUC_1029** | 0.17 | 0.22 | 0.11 | 0.06 | 0.11 | 0.12 | 0.10 | 0.11 |
| **HUC_1304** | 0.04 | 0.04 | 0.02 | 0.02 | 0.08 | 0.08 | 0.08 | 0.08 |
| **HUC_1601** | 0.31 | 0.38 | 0.80 | 0.59 | 0.05 | 0.05 | 0.01 | 0.01 |
| **HUC_1708** | 0.32 | 0.33 | 0.34 | 0.33 | 0.15 | 0.15 | 0.08 | 0.08 |
| **HUC_1711** | 0.15 | 0.17 | 0.12 | 0.11 | 0.17 | 0.17 | 0.14 | 0.15 |
| **HUC_1805** | 0.23 | 0.24 | 0.10 | 0.10 | 0.25 | 0.26 | 0.21 | 0.21 |
| **HUC_1808** | 0.20 | 0.20 | 0.13 | 0.12 | 0.09 | 0.09 | 0.07 | 0.07 |
| **Median** | 0.24 | 0.33 | 0.34 | 0.27 | 0.16 | 0.15 | 0.09 | 0.09 |
| **Difference** | | 0.09 | | 0.07 | | -0.01 | | 0.00 |
| **Change (%)** | | 37.5 | | -20.6 | | -6.3 | | 0.0 |

574

575

Legend: GFPlain90 | Global NFWs | Both wetland sources | NLCD non-floodplain wetlands

576
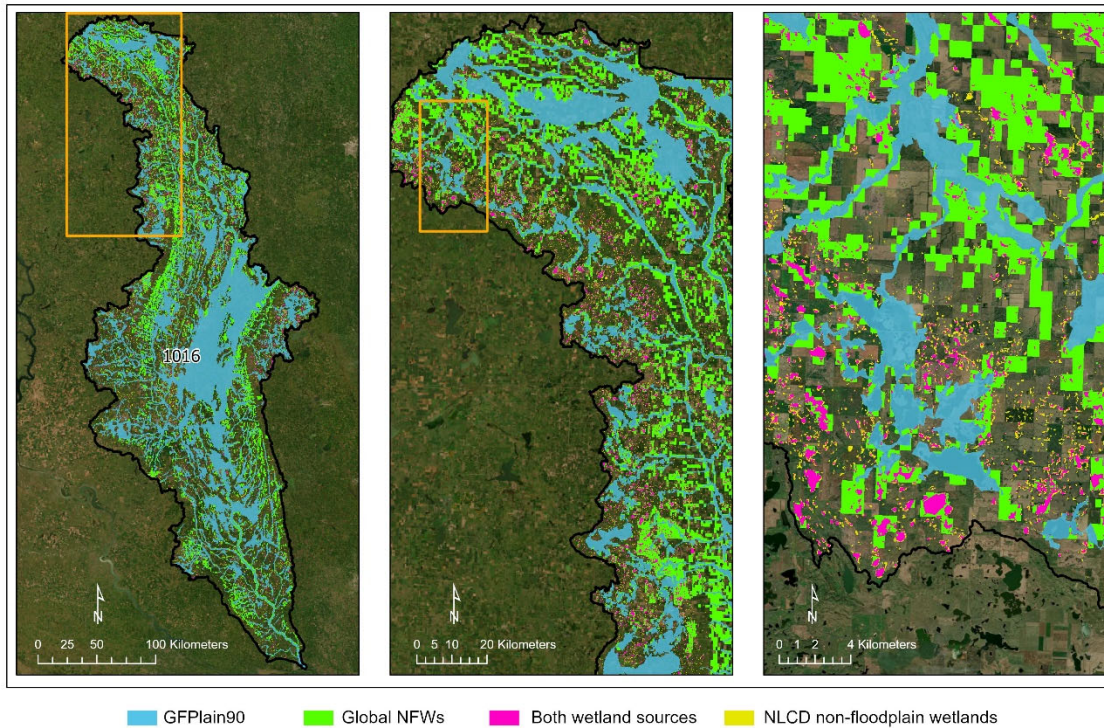
**Figure 4.** Demonstration of the relative accuracy of the Global NFWs in identifying non-floodplain wetlands using a

Prairie Pothole Region watershed (HUC_1016, see Fig. 2) replete with abundant non-floodplain wetlands. Correctly

identified wetlands occur in both wetland sources (magenta color). Omission errors (NLCD non-floodplain

wetlands, smaller systems in yellow) and commission errors (Global NFWs, green) are evident as a result of the

higher resolution of the NLCD validation dataset. Satellite imagery ~~is~~ sourced from ESRI (2022). Note the scale

~~increasing~~increasing from left panel to right panel (i.e., the orange box in the first panel is shown in the second panel

at a higher resolution, and the box in the second panel is shown in the last panel at an even higher resolution). ~~.~~

584    **Table 4.** Non-floodplain wetland performance metrics contrasting both the Global NFWs (abbreviated here as

585    GNFW) and CW-WTD (abbreviated here as WTD, Tootchi et al., 2019) non-floodplain wetland spatial data with the

586    benchmark NLCD wetlands (Dewitz, 2019). Descriptions of the metrics are the same as in Table 3, though the focus

587    here is on wetlands outside the GFPlain90-derived floodplain.

| Hydrologic Unit Code (HUC) ID | Hit Rate (Eq. 1) | | Precision (Eq. 2) | | False Alarm (Eq. 3) | | Critical Success Index (Eq. 4) | |
|---|---|---|---|---|---|---|---|---|
| | WTD | GNFW | WTD | GNFW | WTD | GNFW | WTD | GNFW |
| HUC_0101 | 0.24 | 0.25 | 0.43 | 0.45 | 0.57 | 0.55 | 0.18 | 0.19 |
| HUC_0103 | 0.17 | 0.18 | 0.30 | 0.32 | 0.70 | 0.68 | 0.12 | 0.13 |
| HUC_0106 | 0.15 | 0.18 | 0.14 | 0.17 | 0.86 | 0.83 | 0.08 | 0.10 |
| HUC_0203 | 0.12 | 0.13 | 0.20 | 0.23 | 0.80 | 0.77 | 0.08 | 0.09 |
| HUC_0208 | 0.14 | 0.16 | 0.34 | 0.41 | 0.66 | 0.59 | 0.11 | 0.13 |
| HUC_0304 | 0.26 | 0.28 | 0.45 | 0.49 | 0.55 | 0.51 | 0.20 | 0.21 |
| HUC_0313 | 0.21 | 0.23 | 0.35 | 0.40 | 0.65 | 0.60 | 0.15 | 0.17 |
| HUC_0501 | 0.05 | 0.07 | 0.32 | 0.41 | 0.68 | 0.59 | 0.05 | 0.06 |
| HUC_0706 | 0.05 | 0.06 | 0.63 | 0.72 | 0.37 | 0.28 | 0.05 | 0.05 |
| HUC_0804 | 0.30 | 0.31 | 0.51 | 0.55 | 0.49 | 0.45 | 0.23 | 0.25 |
| HUC_1003 | 0.04 | 0.07 | 0.13 | 0.21 | 0.87 | 0.79 | 0.03 | 0.05 |
| HUC_1015 | 0.07 | 0.25 | 0.05 | 0.28 | 0.95 | 0.72 | 0.03 | 0.15 |
| HUC_1016 | 0.07 | 0.11 | 0.31 | 0.53 | 0.69 | 0.47 | 0.06 | 0.10 |
| HUC_1024 | 0.02 | 0.04 | 0.18 | 0.41 | 0.82 | 0.59 | 0.02 | 0.04 |
| HUC_1029 | 0.03 | 0.06 | 0.25 | 0.58 | 0.75 | 0.42 | 0.03 | 0.06 |
| HUC_1304 | 0.00 | 0.00 | 0.26 | 0.33 | 0.74 | 0.67 | 0.00 | 0.00 |
| HUC_1601 | 0.05 | 0.09 | 0.07 | 0.16 | 0.93 | 0.84 | 0.03 | 0.06 |
| HUC_1708 | 0.06 | 0.06 | 0.33 | 0.35 | 0.67 | 0.65 | 0.05 | 0.05 |
| HUC_1711 | 0.04 | 0.05 | 0.22 | 0.27 | 0.78 | 0.73 | 0.04 | 0.05 |
| HUC_1805 | 0.06 | 0.07 | 0.27 | 0.30 | 0.73 | 0.70 | 0.05 | 0.06 |
| HUC_1808 | 0.05 | 0.06 | 0.25 | 0.36 | 0.75 | 0.64 | 0.04 | 0.06 |
| **Median** | 0.06 | 0.09 | 0.27 | 0.36 | 0.73 | 0.64 | 0.05 | 0.06 |
| **Difference** | | 0.03 | | 0.09 | | -0.09 | | 0.01 |
| **Change (%)** | | 50.0 | | 33.3 | | -12.3 | | 20.0 |

588

589

 **Table 4.** (Continued)

| Hydrologic Unit Code (HUC) ID | F1 (Eq. 5) | | Error Bias (Eq. 6) | | Mean Absolute Error (Eq. 7) | | Aggregate Error Bias (Eq. 8) | |
|---|---|---|---|---|---|---|---|---|
| | WTD | GNFW | WTD | GNFW | WTD | GNFW | WTD | GNFW |
| HUC_0101 | 0.31 | 0.32 | 0.41 | 0.39 | 0.16 | 0.16 | 0.08 | 0.09 |
| HUC_0103 | 0.21 | 0.23 | 0.48 | 0.46 | 0.14 | 0.14 | 0.06 | 0.06 |
| HUC_0106 | 0.14 | 0.18 | 1.11 | 1.03 | 0.11 | 0.11 | -0.01 | 0.00 |
| HUC_0203 | 0.15 | 0.17 | 0.53 | 0.51 | 0.09 | 0.09 | 0.03 | 0.03 |
| HUC_0208 | 0.20 | 0.23 | 0.32 | 0.28 | 0.10 | 0.10 | 0.07 | 0.07 |
| HUC_0304 | 0.33 | 0.35 | 0.44 | 0.40 | 0.17 | 0.17 | 0.08 | 0.09 |
| HUC_0313 | 0.27 | 0.29 | 0.51 | 0.45 | 0.12 | 0.12 | 0.05 | 0.06 |
| HUC_0501 | 0.09 | 0.11 | 0.12 | 0.10 | 0.09 | 0.09 | 0.07 | 0.08 |
| HUC_0706 | 0.09 | 0.10 | 0.03 | 0.02 | 0.09 | 0.09 | 0.09 | 0.09 |
| HUC_0804 | 0.38 | 0.40 | 0.43 | 0.37 | 0.13 | 0.13 | 0.07 | 0.07 |
| HUC_1003 | 0.07 | 0.10 | 0.32 | 0.26 | 0.02 | 0.03 | 0.01 | 0.01 |
| HUC_1015 | 0.06 | 0.26 | 1.46 | 0.85 | 0.03 | 0.02 | -0.01 | 0.00 |
| HUC_1016 | 0.11 | 0.19 | 0.17 | 0.11 | 0.15 | 0.15 | 0.12 | 0.13 |
| HUC_1024 | 0.03 | 0.07 | 0.09 | 0.06 | 0.05 | 0.05 | 0.04 | 0.05 |
| HUC_1029 | 0.05 | 0.11 | 0.09 | 0.05 | 0.08 | 0.08 | 0.07 | 0.07 |
| HUC_1304 | 0.00 | 0.01 | 0.01 | 0.01 | 0.06 | 0.06 | 0.05 | 0.06 |
| HUC_1601 | 0.05 | 0.11 | 0.68 | 0.50 | 0.02 | 0.02 | 0.00 | 0.01 |
| HUC_1708 | 0.10 | 0.10 | 0.12 | 0.12 | 0.11 | 0.11 | 0.09 | 0.10 |
| HUC_1711 | 0.07 | 0.09 | 0.16 | 0.15 | 0.09 | 0.09 | 0.07 | 0.07 |
| HUC_1805 | 0.10 | 0.11 | 0.18 | 0.17 | 0.10 | 0.10 | 0.07 | 0.07 |
| HUC_1808 | 0.08 | 0.11 | 0.15 | 0.12 | 0.02 | 0.02 | 0.01 | 0.01 |
| Median | 0.10 | 0.11 | 0.32 | 0.26 | 0.09 | 0.09 | 0.07 | 0.07 |
| Difference | | 0.01 | | -0.06 | | 0.00 | | 0.00 |
| Change (%) | | 10.0 | | -18.8 | | 0.0 | | 0.0 |

591

592 ~~decrease in False Alarms and a 19 % decrease in Error Bias). There was no difference between the~~

593 ~~datasets with median values for Mean Absolute Error (median values for both = 0.09) or Aggregate Error~~

594 ~~Bias (median values for both = 0.07). Thus, at the 1 km² cell size, there was <10 % difference between~~

595 ~~both the CW-WTD and the Global NFWs and the benchmark NLCD non-floodplain wetlands and open~~

596 ~~waters (with the difference mostly stemming from an increase in identified wetlands with both CW-WTD~~

597 ~~and Global NFWs, as indicated with the positive Aggregate Error Bias values).~~

598

599    **3.3    Global extent analyses and synthesis**

600

601    **3.3.1    Floodplains**

602

603    Floodplains were estimated to cover 26.6 million km$^2$ (Table 5), or 19.7 % of the global landmass.

604    Approximately 23-24 % of the African and Australasian land masses were categorized as occurring

605    within a floodplain, the greatest percentage of global areas so categorized. Conversely, the Arctic

606    (northern Canada and Alaska) and Greenland (excluding the ice sheet) had the least land mass categorized

607    as floodplain (13-14 %). In comparison, Nardi et al. (2019) calculated a global floodplain extent of

608    13,394,139 km$^2$, using a 250-m pixel size, a 1000 km$^2$ minimum contributing area, and bounding their

609    study between 60$^\circ$ N and 60$^\circ$ S latitudes. Our analyses using the same latitudinal bounds but with a higher

610    resolution dataset (90 m) and a 20 km$^2$ minimum contributing area identified 24,185,775 km$^2$, an 81 %

611    areal increase (Fig. B1). The relative percent composition of each HydroBASIN that is comprised of

612    GFPlain90 floodplains is given in Fig. 5.

613
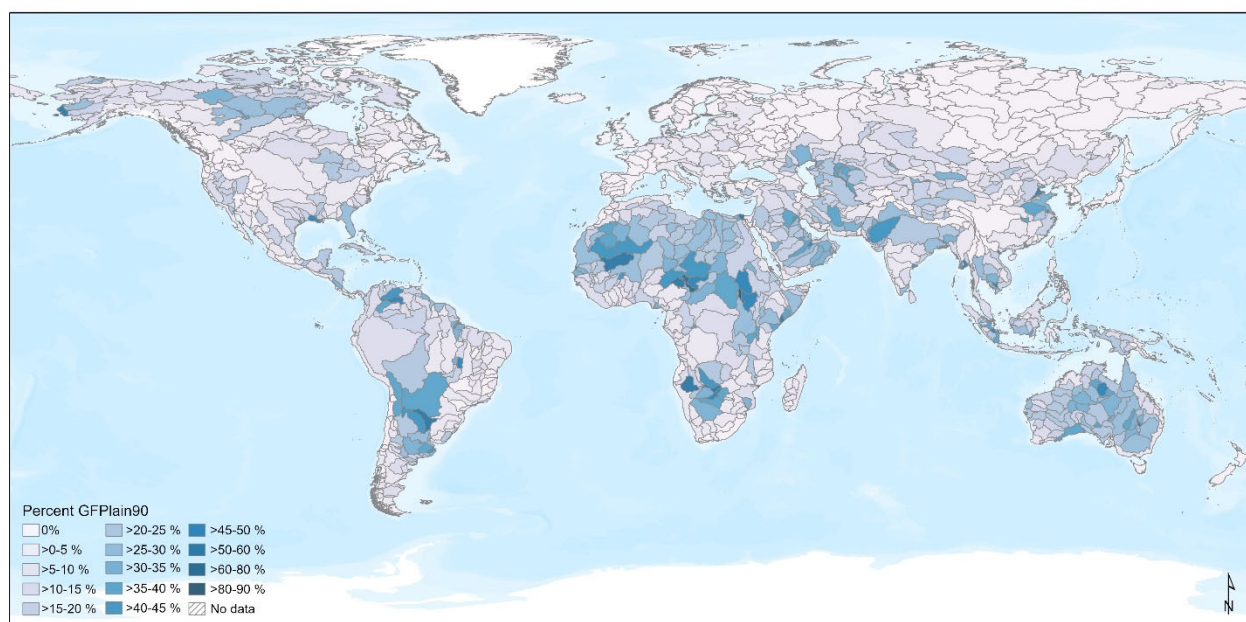
614

615     **Figure 5.** Floodplain extents derived from GFPlain90 as a proportion of each of the Level 4 HydroBASINS

616     (Lehrner and Grill, 2013). The data range demonstrated that up to ~90 % of a given watershed was comprised of

617     floodplain area, as evidenced by HydroBASINS in south central Africa and central South America. The basemap

618     layer is the ESRI World Terrain Base (2022).

619

620

621

**Table 5.** Calculated floodplain area for each HydroBASINS at the global scale. Our analyses found 19.7 % of the

landmass occurs within a floodplain.

| HydroBASINS Region | Floodplain (km²) | Floodplain Percent of Landmass |
|---|---|---|
| Africa | 6,990,859 | 23.3 % |
| Arctic (northern Canada & Alaska) | 894,594 | 14.2 % |
| Asia | 4,283,991 | 20.6 % |
| Australasia | 2,649,395 | 23.8 % |
| Europe and Middle East | 3,415,308 | 19.1 % |
| Greenland (excl. ice sheet) | 270,813 | 12.6 % |
| North & Central America (excl. Alaska) | 2,713,346 | 17.0 % |
| Siberian Russia | 2,051,305 | 15.8 % |
| South America | 3,368,778 | 18.9 % |
| Total | 26,638,389 | 19.7 % |

624

625

### 3.3.2 Wetlands

627

Global Wetland extent covered 30.5 million km² (Table 6). With a focus on smaller systems compared to

those presented by Tootchi et al. (2019), our Global Wetland dataset identified 11-% more potential

global wetlands (3 million km² additional wetlands).

631

Australasia had the greatest proportional wetland abundance (see also Zhu et al., 2022), with wetlands

covering 38 % of the landmass (driven, in part, by island abundance and fringing estuarine wetlands [Fan

et al., 2013]). Greenland (3 %) and Africa (12 %) had the least wetlands identified on the land mass.

635

**Table 6.** Estimated Global Wetlands areal extent for each of the nine regional HydroBASINS (Lehner and Grill,

2013). As described in the text, Global Wetlands extent incorporates the CW-WTD (Tootchi et al., 2019), CCI

(Herold et al., 2015), and GSW (Pekel et al., 2016); lakes of ≥ 10 ha have been removed (Messager et al., 2016).

| HydroBASINS Region | Wetlands (km²) | Wetland Percent of Landmass |
|---|---|---|
| Africa | 3,524,917 | 11.8 % |
| Arctic (northern Canada & Alaska) | 1,807,830 | 28.6 % |
| Asia | 5,543,333 | 26.6 % |

| | | |
|---|---|---|
| **Australasia** | 4,283,996 | 38.4 % |
| **Europe and Middle East** | 2,465,074 | 13.8 % |
| **Greenland (excl. ice sheet)** | 60,761 | 2.8 % |
| **North & Central America (excl. Alaska)** | 4,107,333 | 25.8 % |
| **Siberian Russia** | 3,578,868 | 27.6 % |
| **South America** | 5,140,139 | 28.8 % |
| **Total** | 30,512,251 | 22.6 % |

639

640

### 3.3.3    Non-floodplain wetlands (Global NFW)

642

Approximately 16.0 million km$^2$ of potential non-floodplain wetlands were identified globally (Global

NFWs, Fig. 56), meaning that 11.9 % of the global landmass is estimated to be covered by non-floodplain

wetlands (Table 7). This represents ~53 % of the total global wetlands found in the dataset used in this

analysis (see Methods: Wetland Data, above). The global distribution of non-floodplain wetlands is

widespread, though they were found to comprise a higher proportion of wetlands within more northern

HydroBASINS watersheds (i.e., higher abundances in formerly glaciated basins), as demonstrated in Fig.

67. The Arctic portion of northern Canada and Alaska (21.7 %), and Siberian Russia (17.4 %), typically

underlain by permafrost and frequently inundated or saturated due to poor drainage evolution

(Kremenetski et al., 2003; Robarts et al., 2013; Olefeldt et al., 2021), had the greatest percent non-

652

653
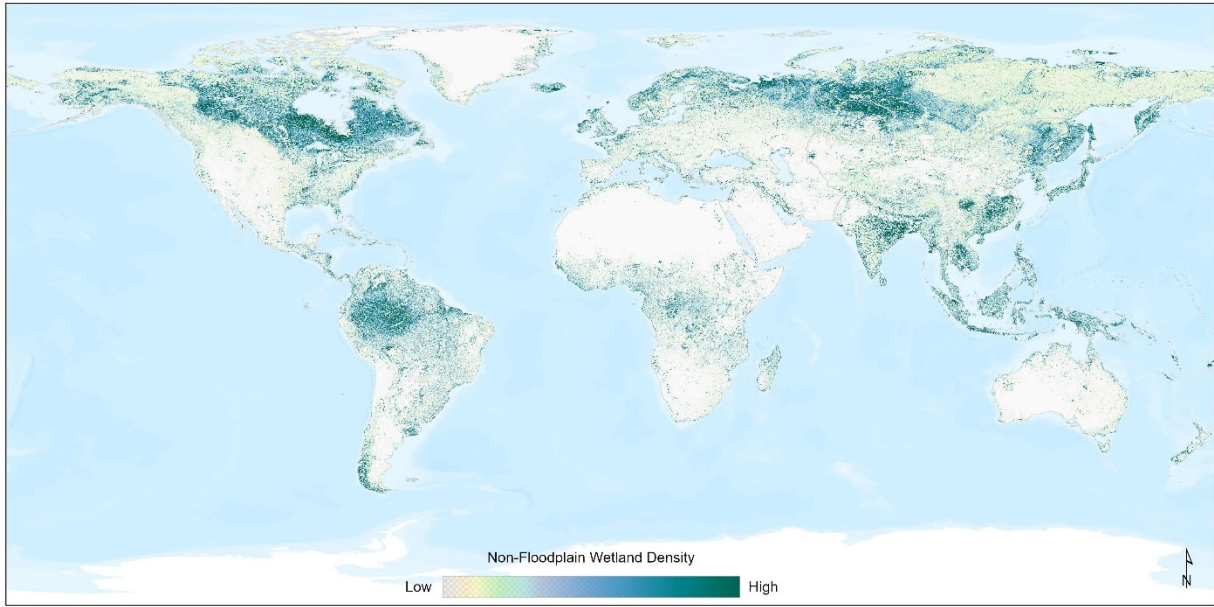
654 **Figure ~~5~~6.** Non-floodplain wetlands, Global NFWs, are found worldwide, with a greater abundance in formerly

655 glaciated landscapes of northern climates (e.g., northern North America and Siberian Russia) as well as within the

656 Amazon basin (South America). This density map was created using the Focal Statistics tool in ArcGIS Pro 2.9.1.

657 The basemap layer is the ESRI World Terrain Base (2022).

658

659

660

661

662
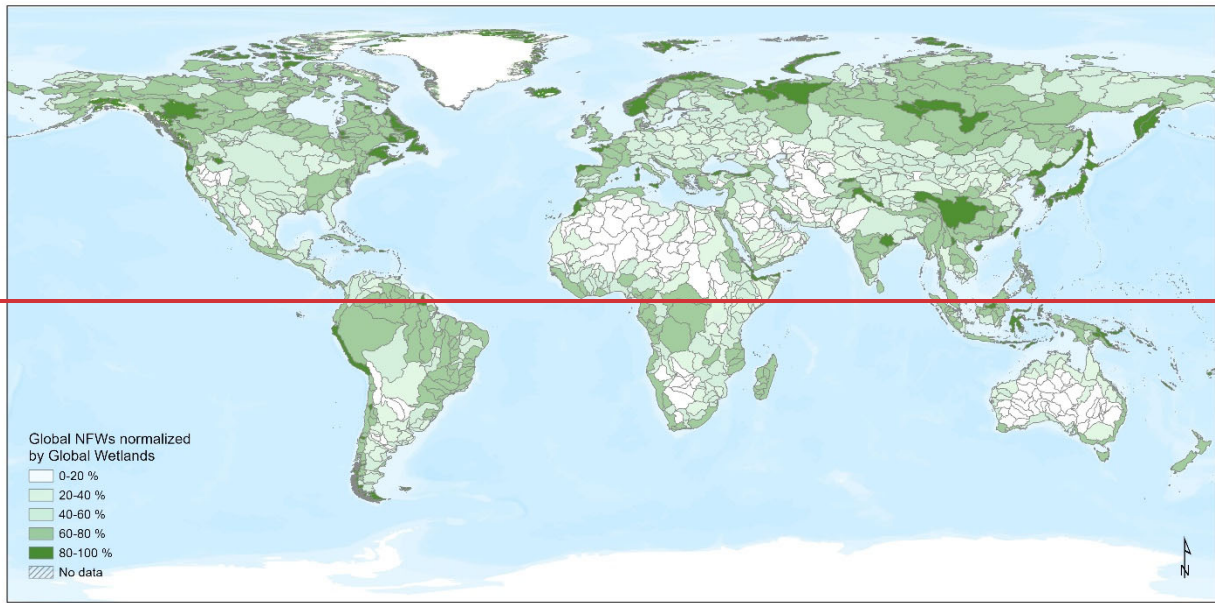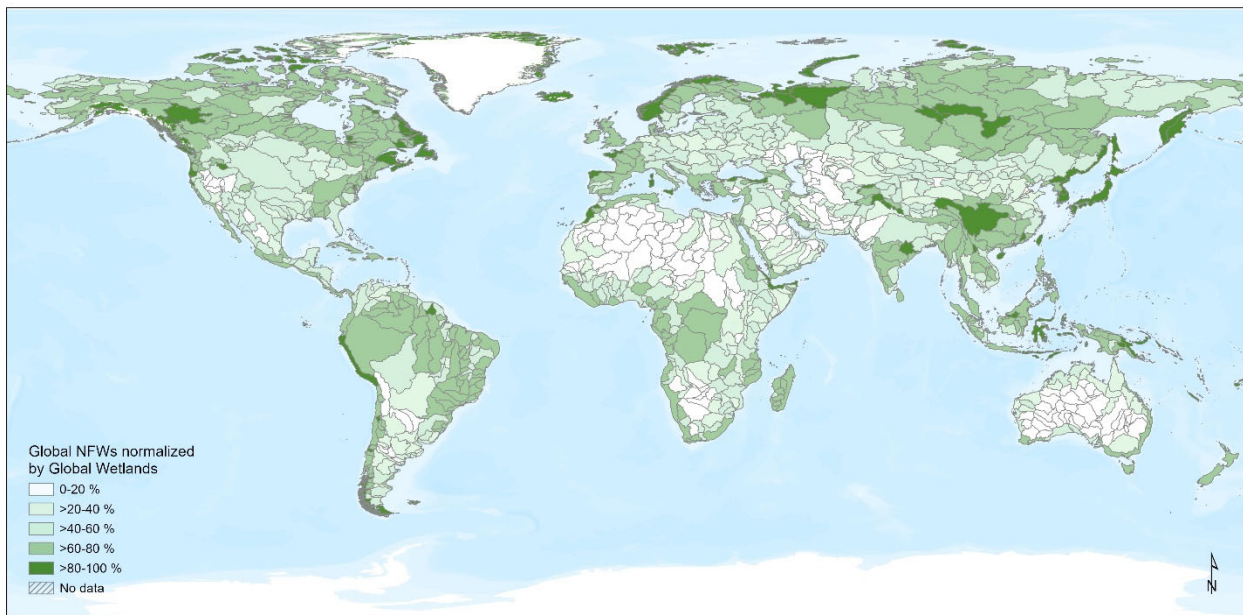
**Figure 6̶7.** The proportion of non-floodplain wetlands, Global NFWs, within a given HydroBASINS watershed (Lehrner and Grill, 2013), ranging up to 100 %, varied globally. The impacts or effects of non-floodplain wetlands on biological, biogeochemical, and hydrological functions will vary based on their relative abundance, location within the watershed, and hydrologic characteristics (Lane et al., 2018). The basemap layer is the ESRI World Terrain Base (2022).

668

669

670    floodplain wetlands. Africa (5.4 %) and Greenland (1.0 %, excluding ice sheets) had the least abundance

671    of non-floodplain wetlands. A four-direction region-group (contagion) analysis conducted to identify

672    adjacent pixels considered as contiguous units or non-floodplain wetland systems identified 32.8 million

673    individual non-floodplain wetlands. Non-floodplain wetlands are typically small aquatic systems (see

674    Table 7): the median size differed across the HydroBASINS regions from 0.018 $km^2$ (1.8 ha) to 0.138

675    $km^2$ (13.8 ha) with a global median of 0.039 $km^2$ (3.87 ha).

**Table 7.** Global NFW data further described by HydroBASINS region.

| HydroBASINS Region | Global NFW Extent (km²) | Count of Global NFWs (#) | Global NFW Percent of Landmass | Global NFW Median Area (km²) |
|---|---|---|---|---|
| Africa | 1,611,225 | 2,698,465 | 5.4 % | 0.138 |
| Arctic (northern Canada & Alaska) | 1,371,937 | 5,956,081 | 21.7 % | 0.018 |
| Asia | 2,924,900 | 4,564,172 | 14.0 % | 0.049 |
| Australasia | 850,402 | 1,448,315 | 7.6 % | 0.054 |
| Europe and Middle East | 1,475,355 | 3,740,961 | 8.3 % | 0.054 |
| Greenland (excl. ice sheet) | 21,747 | 180,726 | 1.0 % | 0.018 |
| North & Central America (excl. Alaska) | 2,608,158 | 5,740,066 | 16.4 % | 0.025 |
| Siberian Russia | 2,255,689 | 4,864,577 | 17.4 % | 0.063 |
| South America | 2,891,604 | 3,572,294 | 16.2 % | 0.096 |
| Total | 16,011,018 | 32,765,657 | 11.9 % | 0.039 |

## 4     Discussion

We report here for the first time the global abundance of non-floodplain wetlands, a functionally important and imperiled resource (Creed et al., 2017). Our estimate of 16.0 million km² suggests that approximately 53 % of the ~~global population of~~Earth's wetlands are likely non-floodplain wetland systems. These aquatic systems are small, with a range from 0.018-0.138 km² (1.8-13.8 ha) across the globe and a global median size of 0.039 km² (3.87 ha, see Table 7).

The global abundance of non-floodplain wetlands is a reasonable first approximation of the total non-floodplain wetland extent. For instance, non-floodplain wetland estimates in the CONUS were conducted by Lane et al. (2022) using high-resolution aerial-sourced spatial data layers developed by the National Wetlands Inventory (U.S. Fish and Wildlife Service, various dates). Lane et al. (2022) reported approximately 23% of the area of freshwater wetlands to be non-floodplain wetland systems. Yet the CONUS has lost nearly half of its wetlands since the European colonization (Dahl, 1990), with smaller and shallower non-floodplain wetlands likely being disproportionately lost (Van Meter and Basu, 2015; Serran et al., 2017).

695   Tootchi et al. (2019) – our base input geospatial data layer – calculated that the global wetland extent

696   identified from incorporating both regularly flooded wetland systems (surface-water and precipitation-

697   sourced) and groundwater-driven wetland systems (e.g., Fan et al., 2013; Hu et al., 2017b) resulted in

698   approximately 27.5 million $km^2$ of wetlands, a value towards the higher-end of previously published

699   geospatial wetland datasets (Hu et al., 2017a). In their synthesis, Tootchi et al. (2019) explained their

700   values as particularly influenced by groundwater-driven wetlands, especially those in the tropics ($10^o$ N-

701   $10^o$ S latitudes, Zhu et al., 2022), following recent studies acknowledging the under-estimation of those

702   wetland systems (e.g. Wania et al., 2013; Gumbricht et al., 2017).

703

704   It follows that incorporating additional higher-resolution satellite inundation data (Pekel et al., 2016) as

705   well as groundwater-driven wetland systems data (e.g., Fan et al., 2013; Tootchi et al., 2019), as

706   conducted in this study, would similarly maintain the trend towards the higher end in global estimates as

707   found by Hu et al. (2017a) and Toochi et al. (2019). This is meted out in the simple contrast between the

708   proportional abundance of non-floodplain wetland systems identified here against the 30 m NLCD data

709   product described above (Dewitz, 2019) across the 21 CONUS watersheds in this study. The calculated

710   median watershed abundance of non-floodplain wetlands in both the Global NFWs (9.4 %) and the

711   Tootchi et al. (2019) CW-WTD (9.1 %) datasets from our validation watersheds are nearly 5-fold the

712   abundance of the benchmark data from the NLCD (Table 78). However, this is contrasted with a 7-fold

713   *under-representation* of non-floodplain wetlands as derived from the satellite based GSW data (Table 8,

714   Pekel et al., 2016). This suggests that our first approximation of global non-floodplain wetland estimates

715   may be high, primarily due to the resolution of the input data layers. However, as we discuss below,

716   additional factors than just resolution are likely at play.

717

718   It is apparent that the GSW alone is insufficient to map non-floodplain wetlands (this study, Vanderhoof

719   and Lane, 2019). Though useful as a satellite-based input data layer, the GSW by itself appears

720   inadequate for identifying non-floodplain wetlands because it relies on surface-water inundation and

721     ignores saturated wetland systems and those driven by groundwater discharge and upwelling (Winter et

722     al., 1998). Fan et al. (2013) found that groundwater drivers of aquatic system state were important and

723     underrepresented in global datasets. Relying on surface water inundation captured during satellite

724     overflights depends not only on an unobstructed view of the waterbody (e.g., not obscured by trees) but

725     also fortuitous timing regarding inundation status. For example, in an analysis of non-floodplain wetlands

726     of the CONUS as derived by distance from an aquatic system, Lane and D'Amico (2016) reported that

727     just over 50 % of the non-floodplain wetlands were classified as seasonally or temporarily flooded –

728     meaning that cloud-free and unobscured overflights would only potentially identify these systems at

729

730     **Table 8.** A comparison of the non-floodplain wetland distribution within the 21 HUCs contrasting across NLCD

731     (the benchmark data layer, Dewitz, 2019), Global NFW (this study), CW-WTD (Tootchi et al., 2019), and GSW

732     (Pekel et al., 2016). The CW-WTD (at 500 m) and the Global NFW (coupling 500 m, 300 m, and 30 m data),

733     derived from the CW-WTD, identified 5-fold the abundance of non-floodplain wetlands whereas the GSW under-

734     estimated non-floodplain wetlands nearly 7-fold.

| HUC ID | Percent HUC as NLCD NFW | Percent HUC as Global NFW | Percent HUC as CW-WTD NFW | Percent HUC as GSW NFW |
|---|---|---|---|---|
| HUC_0101 | 10.4 % | 19.2 % | 18.9 % | 0.1 % |
| HUC_0103 | 8.1 % | 14.6 % | 14.3 % | 0.2 % |
| HUC_0106 | 8.2 % | 8.0 % | 7.5 % | 0.3 % |
| HUC_0203 | 4.9 % | 8.4 % | 8.3 % | 0.4 % |
| HUC_0208 | 4.7 % | 12.0 % | 11.5 % | 4.6 % |
| HUC_0304 | 12.2 % | 21.7 % | 20.8 % | 12.2 % |
| HUC_0313 | 8.3 % | 14.4 % | 13.5 % | 8.2 % |
| HUC_0501 | 1.5 % | 9.2 % | 8.9 % | 0.1 % |
| HUC_0706 | 0.7 % | 9.7 % | 9.5 % | 0.3 % |
| HUC_0804 | 9.7 % | 17.1 % | 16.2 % | 9.7 % |
| HUC_1003 | 0.7 % | 2.1 % | 1.9 % | 0.2 % |
| HUC_1015 | 1.8 % | 2.0 % | 1.3 % | 0.1 % |
| HUC_1016 | 3.6 % | 16.6 % | 15.5 % | 2.6 % |
| HUC_1024 | 0.5 % | 5.1 % | 4.9 % | 0.2 % |
| HUC_1029 | 0.9 % | 8.4 % | 7.7 % | 0.4 % |
| HUC_1304 | 0.0 % | 5.5 % | 5.5 % | 0.0 % |
| HUC_1601 | 0.7 % | 1.3 % | 1.0 % | 0.1 % |
| HUC_1708 | 2.0 % | 11.7 % | 11.6 % | 0.4 % |
| HUC_1711 | 1.8 % | 9.4 % | 9.1 % | 0.2 % |
| HUC_1805 | 2.2 % | 9.9 % | 9.7 % | 0.5 % |
| HUC_1808 | 0.3 % | 1.7 % | 1.6 % | 0.1 % |
| **Median** | 2.0 % | 9.4 % | 9.1 % | 0.3 % |

735

736 ~~underrepresented in global datasets. Relying on surface-water inundation captured during satellite~~

737 ~~overflights depends not only on an unobstructed view of the waterbody (e.g., not obscured by trees) but~~

738 ~~also fortuitous timing regarding inundation status. For example, in an analysis of non-floodplain wetlands~~

739 ~~of the CONUS as derived by distance from an aquatic system, Lane and D'Amico (2016) reported that~~

740 ~~just over 50 % of the non-floodplain wetlands were classified as seasonally or temporarily flooded –~~

741 ~~meaning that cloud-free and unobscured overflights would only potentially identify these systems at~~

742 certain inundated times of the year. Additionally, Lane and D'Amico (2016) identified another 6 % of

743 CONUS non-floodplain wetlands as saturated (i.e., wetlands with saturated substrates but with surface

744 water seldom present). These wetlands would not be identified by the GSW (Pekel et al., 2016) resulting

745 in a further under-representation of the global resource. Similarly, Hamunyela et al. (2022), analyzing

746 ~150,000 km$^2$ in southeastern Africa, found that the GSW underestimated surface water extent (i.e.,

747 omission errors) by nearly 65%. Vanderhoof and Lane (2019) found approximately 42% omission rates

748 when contrasting the GSW data to surface-water extent in non-floodplain wetlands ranging from 0.2-17.6

749 ha in area in the Midwestern US. While the GSW is an outstanding dataset that is continuing to be

750 managed and updated, the GSW and its derived product have limitations in their stand-alone utility in

751 global non-floodplain wetland analyses.

752

753 While solely using satellite-based surface-water data products omits groundwater-driven and saturated

754 wetlands and likely results in non-floodplain wetland underestimations, our Global Wetland data

755 incorporated the finer-resolution CCI (Herold et al., 2015) and GSW (Pekel et al., 2016) products into the

756 Tootchi et al. (2019) base map, substantially improving ~~the~~ wetland identification ~~of non-floodplain~~

757 ~~wetlands~~ (see Table 3). These improvements, as indicated by performance indices increasing from 10-50

758 % in the derived Global ~~Wetland~~ NFW data (see Table ~~4~~4), support the inclusion of these higher-

759 resolution satellite-based data (Herold et al., 2015; Pekel et al., 2016) with groundwater datasets (Fan et

760 al., 2013), especially when focused on smaller and non-floodplain wetland systems. Similarly, at a coarser

761 scale of 1 km, there was a difference in Mean Absolute Error value of 0.09 (see Table 4) between the

762   Global NFWs and the benchmark NLCD. This ~9 % difference between the two datasets at a 1 km

763   resolution (the former originating at 500 m and the latter at 30 m) further suggest substantive potential

764   utility in these global non-floodplain wetland data for effective natural resource management and

765   decision-making.

766

767

## 5    Implications

Non-floodplain wetlands remain vulnerable waters (Creed et al., 2017), despite the fact that the hydrological, biogeochemical, and biological functions performed by non-floodplain wetlands are increasingly noted in the literature (e.g., Leibowitz, 2003; Creed et al., 2017; Lane et al., 2018; Lane et al., 2022), incorporated into eco-hydrological models by the scientific community (e.g., Fossey and Rousseau, 2016; Golden et al., 2017; Golden et al., 2021; Leibowitz et al., ~~In Review~~2023), and considered by policy makers (e.g., Biggs et al., 2017; Drenkhan et al., 2022). Their global fate has important implications for watershed-scale resilience to changing climatic conditions (Mckenna et al., 2017; Lane et al., 2022) affecting the measured benefits humans receive from biogeochemical processing, stormwater attenuation, and drought mitigation functions provided by non-floodplain wetlands.

Global attention to functions of non-floodplain wetlands has increased in the United States (Marton et al., 2015; Rains et al., 2016; Cohen et al., 2016), Europe (Biggs et al., 2017; Nitzsche et al., 2017; Rodríguez-Rodríguez et al., 2021), Asia (Kam, 2010; Van Meter et al., 2014), Australia (Adame et al., 2019), Africa (Merken et al., 2015; Samways et al., 2020), South America (Rodrigues et al., 2012; Cunha et al., 2019) and elsewhere (see extensive review in Chen et al., 2022). This includes analyses of non-floodplain wetlands both as individual systems (e.g., assessing the functions of a single wetland or wetland complex; Badiou et al., 2018) as well as agglomerated, watershed-scale functioning systems (e.g., answering questions on the functional contributions of all non-floodplain wetlands at larger spatial extents; Golden et al., 2016; Blanchette et al., 2022). Previous studies found that non-floodplain wetlands are overwhelmingly important contributors to biogeochemical and hydrological functions affecting downgradient (i.e., down-stream) water quality and streamflow (e.g., McLaughlin et al., 2014; Marton et al., 2015; Cohen et al., 2016; Rains et al., 2016; Golden et al., 2019; Cheng et al., 2020). Hence, with the development of this publicly available dataset, and subsequent improvements by others, it is hoped that

793  these important aquatic systems will be incorporated into resource management and decision-making

794  across the globe.

795

796  Recently, Lane et al. (2022) identified global-scale geospatial data of the spatial extent and spatial

797  configuration of vulnerable waters – non-floodplain wetlands and headwater stream systems (e.g.,

798  ephemeral, intermittent, and perennial low-order waters [Strahler, 1957]) – as a critical scientific gap.

799  Discounting their significance in watershed-scale hydrology and nutrient biogeochemistry analyses – as

800  well as their importance in biological processes (Schofield et al., 2018; Smith et al., 2019; Mushet et al.,

801  2019) – affects quantification of the myriad ecosystem services they provide (De Groot, 2006; Colvin et

802  al., 2019). For instance, Golden et al. (2021) provide a tangible example of the functional effects and

803  influence of non-floodplain wetlands once incorporated into watershed-scale hydrologic models (Fig. ~~7~~8):

804  ignoring non-floodplain wetlands in the model resulted in projected critical flood-stage return intervals

805  (e.g., 50 yr and 100 yr floods) being reached within a given modeled time frame. Conversely,

806  incorporating non-floodplain wetlands and their storage capacities into a river basin model (e.g., Rajib et

807  al., 2020) demonstrated that non-floodplain wetlands significantly attenuate storm flows, for when non-

808  floodplain wetlands are "…integrated into the model, those simulated *flood stages are not reached*"

809  (Golden et al., 2021, p. 3, emphasis added). The hydrological functions and concomitantly the associated

810  biogeochemical functions (e.g., Marton et al., 2015) of non-floodplain wetlands demand an effective

811  accounting of their spatial extent and configuration, as demonstrated in this novel global dataset.

812

813  **6    Global Non-Floodplain Wetlands: Continuing advancements and conclusion**

814

815  Noting the challenges in accurately identifying non-floodplain wetlands – including small size, frequent

816  non-perennial hydrological inundation, soil saturation rather than overlying surface water, and canopy or

817  cloud cover obstructing satellite or airborne detection – recommendations for advanced analyses of non-

818  floodplain wetland extent hinge initially on the use of ancillary data sources. For instance, global

819 assessments will be improved through wall-to-wall high resolution digital elevation models that are used

820 to identify depressions on the landscape (e.g., Wu et al., 2019b). Though not all landscape depressions are

821 non-floodplain wetlands (or wetlands at all), analyses that include depressions may find improved

822 performance when used in combination with vegetation-based assessments or spectral analyses

823 identifying water (Devries et al., 2017; Evenson et al., 2018b). Similarly, emerging synthetic aperture

824 radar-based landscape classifications (e.g., Huang et al., 2018; Martinis et al., 2022; Brown et al., 2022)

825 and both airborne and satellite-borne hyperspectral and advanced analyses, including LiDAR, as well as

826

827
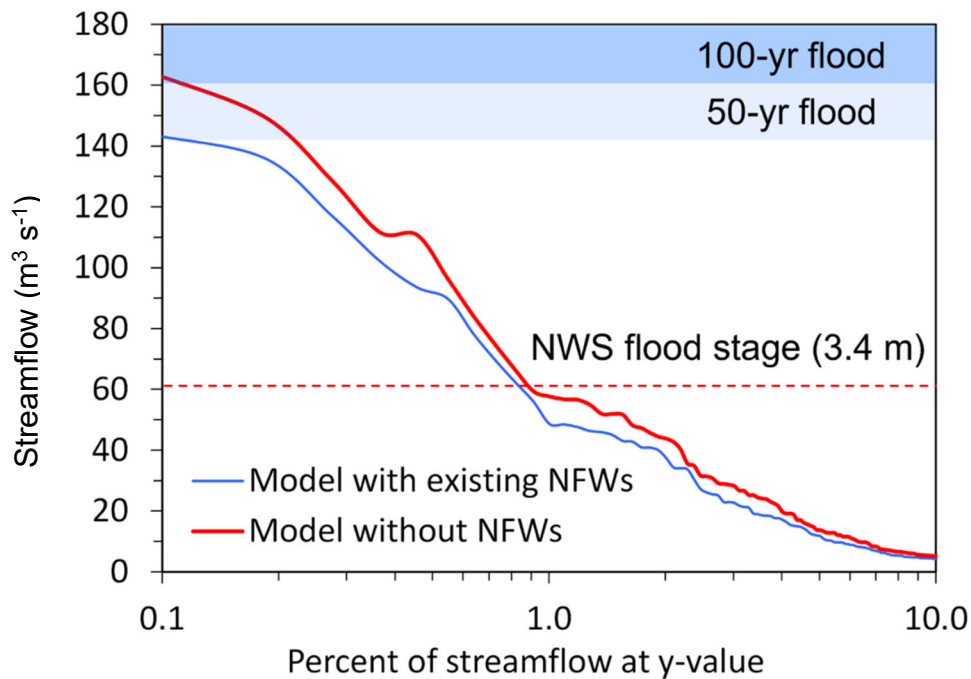
828

829 **Figure 7̶8**. Non-floodplain wetlands attenuate storm flows and decrease flooding hazards. In this example from

830 Golden et al. (2021, used by permission under Creative Commons Attribution 4.0 license), incorporating the

831 floodwater storage and attenuation functions of non-floodplain wetlands (NFWs, here) resulted in substantive

832 decreases in flood-stage heights (i.e., modeled stream outcomes incorporating non-floodplain wetlands reached

833 neither 50 yr nor 100 yr floods extents). The ~~example~~ data from Golden et al. (2021) is of USGS Pipestem Creek

834 gage 06469400, draining approximately 1,800 km$^2$.

analytical capabilities (e.g., machine-learning approaches, object-oriented classifications, Berhane et al., 2018); topographically based models, Xi et al., 2022; see Table B1) hold great promise for improved resolution and performance in identifying non-floodplain wetlands (Christensen et al., 2022).

6        Global Non-Floodplain Wetlands: Continuing advancements and conclusion

Noting the challenges in accurately identifying non-floodplain wetlands—including small size, frequent non-perennial hydrological inundation, soil saturation rather than overlying surface water, and canopy or cloud cover obstructing satellite or airborne detection—recommendations for advanced analyses of non-floodplain wetland extent hinge initially on the use of ancillary data sources. For instance, global assessments will be improved through wall-to-wall high resolution digital elevation models that are used to identify depressions on the landscape (e.g., Wu et al., 2019b). Though not all landscape depressions are non-floodplain wetlands (or wetlands at all), analyses that include depressions may find improved performance when used in combination with vegetation-based assessments or spectral analyses identifying water (Devries et al., 2017; Evenson et al., 2018b). Similarly, emerging synthetic aperture radar-based landscape classifications (e.g., Huang et al., 2018; Martinis et al., 2022; Brown et al., 2022) and both airborne and satellite-borne hyperspectral and advanced analyses, including LiDAR, as well as analytical capabilities (e.g., machine-learning approaches, object-oriented classifications, Berhane et al., 2018); topographically based models, Xi et al., 2022) hold great promise for improved resolution and performance in identifying non-floodplain wetlands (Christensen et al., 2022).

The Global NFW dataset is not perfect, yet it incrementally advances the current understanding of the potential extent of this important aquatic resource. Limitations of the global dataset (see also Section 4) include the error-propagation and imperfections of the input data layers, including the relatively coarse nature of four of the main input data layers (i.e., the 1000 m groundwater data from Fan et al. (2013), 500 m CW-WTD from Tootchi et al. (2019), 500 m GIEMS-D15 from Fluet-Chouinard et al. (2015), and the 300 m CCI from Herold et al. (2015)) relative to the target wetland size as clearly evident in Fig. 4. We

861     additionally acknowledge that omission and commission errors remain within this global data product.

862     For instance, our floodplain-masking process may have inadvertently misassigned pixels derived at 500 m

863     into either non-floodplain or floodplain groups. Though data were not lost when we resampled

864     downwards to 30 m from 500 m, the topological relationships were not necessarily maintained, adding

865     error to the determination of floodplain or non-floodplain pixel status (especially as it relates to those

866     pixels proximate to floodplains). Though imperfect, we suggest Global NFW data should be cautiously

867     incorporated into hydrological, biogeochemical, and biological models to account for the important

868     functions non-floodplain wetlands perform.

869

870     Similarly, though this Global NFW is a static data layer, land use, development, and climate changes

871     continue to affect the prevalence of wetlands worldwide. Fluet-Chouinard et al. (2023) recently noted a

872     global wetland loss of 21% since 1700, with rapid increases from 1950s onwards. Returning to the

873     identification of wetlands and their spatial location vis-à-vis floodplains, using the preponderance of

874     higher-resolution (i.e., < 30 m) and high-return interval sensors will improve both the spatial and

875     temporal accuracy of these data, decreasing commission and omission errors (e.g., Table 8) while

876     increasing the accurate identification of smaller aquatic features that occasional cease to hold standing

877     water.

878

879     The keys to quantifying the functional contributions, ecosystem services, and watershed-scale resilience

880     conferred by non-floodplain wetlands through hydrological, biogeochemical, and biological processes are

881     found through, as a first principle, identifying the spatial extent and configuration of this disappearing and

882     imperiled aquatic system (Creed et al., 2017; Lane et al., 2022). This novel geospatial dataset, freely

883     available (https://gaftp.epa.gov/EPADataCommons/ORD/Global_NonFloodplain_Wetlands/, Lane et al.,

884     2023), provides for sustainable management of an important aquatic resource and advances the global

885     assessment of non-floodplain wetland functions by facilitating non-floodplain wetland inclusion in both

886     existing models and those under development (Golden et al., 2021).

887

## 7      Data availability

889

The data are available on the United State Environmental Protection Agency's Environmental Dataset

Gateway (DOI: https://doi.org/10.23719/1528331, Lane et al., 2023) or

https://gaftp.epa.gov/EPADataCommons/ORD/Global_NonFloodplain_Wetlands/, (last accessed

12/06/2022). Here, we provide global gridded floodplain (90 m, GFPLain90, ~/Global_Floodplains),

global gridded wetlands (30 m, Global Wetlands, ~/Global_Wetlands), and global gridded non-floodplain

wetlands (30 m, Global NFWs, ~/Global_NFWs) for each of the 3142 HydroBASINS, organized by

HydroBASINS region (see, e.g., Table 7).

897

**Author contributions.** CL, JC, HG, and ED conceptualized the study, developed the formal analysis, and

conducted and/or assisted the data validation. CL wrote and edited the manuscript, while JC and HG

reviewed and edited the manuscript. ED also developed the methodology, curated the data, conducted the

formal spatial analysis, validated the data, visualized the data, and reviewed and edited the manuscript.

QW and AR assisted in methodology development, validated the study outputs, conducted formal

analyses, and reviewed and edited the manuscript.

904

**Competing interests.** The corresponding authors have declared that none of the authors have any

competing interests.

907

**Disclaimer.** Publisher's note: Copernicus Publications remains neutral with regard to jurisdictional

claims in published maps and institutional affiliations.

910

**Acknowledgements.** We greatly appreciate the scientific contributions and stimulative discussions in the

papers led by Ardalan Tootchi, Sean Woznicki, Fernando Nardi, Oliver Wing, Paul Bates, and their co-

913  authors that inspired us to complete these analyses. Jeremy Baynes and John Johnston conducted critical

914  reviews to improve this manuscript, and their efforts are acknowledged. This paper has been reviewed in

915  accordance with the US Environmental Protection Agency's peer and administrative review policies and

916  approved for publication. Mention of trade names or commercial products does not constitute

917  endorsement or recommendation for use. Statements in this publication reflect the authors' professional

918  views and opinions and should not be construed to represent any determination or policy of the US

919  Environmental Protection Agency.

920

921  **Review statement.** This paper was edited by [Topical Editor] Yuanzhi Yao and reviewed by Youjiang

922  Shen and Michele Ronco [names/anonymous].

923

924  **Appendix A: Abbreviations**

925  AEB            Aggregate error bias

926  CaMa-Flood     Catchment-based Macro-scale Floodplain

927  CCI            Climate change initiative

928  CIMA-UNEP   CIMA Research Foundation - United Nations Environmental Programme

929  CONUS          Conterminous United States

930  CSI            Critical Success Index

931  CW-WTD         Composite wetland-water table depth

932  DEM            Digital elevation model

933  EB             Error Bias

934  ECMWF          European Centre for Medium-Range Weather Forecasts

935  EPA            Environmental Protection Agency

936  ESA            European Space Agency

937  FA             False Alarm

938  FEMA           Federal Emergency Management Agency

| | | |
|---|---|---|
| 939 | GDW | Groundwwater-driven wetlands |
| 940 | GFPlain | Global Floodplain |
| 941 | GIEMS-D15 | Global Inundation Extent from Multi-Satellites Downscaled - 15 arcseconds |
| 942 | GIS | Geographic information systems |
| 943 | GLOFRIS | Global Flood Risk with Image Scenarios |
| 944 | GLWD | Global Lakes and Wetlands Database |
| 945 | GNFW | Global Non-floodplain wetlands |
| 946 | GSW | Global surface water |
| 947 | GW | Global wetlands |
| 948 | H | Hit Rate |
| 949 | HUC | Hydrologic unit code |
| 950 | IPCC | Intergovernmental Panel on Climate Change |
| 951 | JRC | Joint Research Center |
| 952 | LIDAR | Light detection and ranging |
| 953 | MAE | Mean absolute error |
| 954 | MERIT | Multi-Error Removed Improved Terrain |
| 955 | ML | Machine learning |
| 956 | NFW | Non-floodplain wetland |
| 957 | NLCD | National Land Cover Database |
| 958 | NWS | National Weather Service |
| 959 | P | Precision |
| 960 | RFW | Regularly flooded wetland |
| 961 | SAR | Synthetic aperture radar |
| 962 | USA | United States of America |
| 963 | USGS | United States Geological Survey |
| 964 | UTM | Universal Transverse Mercator |

965     WTD            Water table depth

966

967 **Appendix B: Supplemental Tables and Figures**

968 **Table B1.** Emerging global land cover datasets related to surface water and wetlands.

| Data Set | Resolution | Years of Data | Wetland Classes | Image Sources | Reference and website |
|---|---|---|---|---|---|
| ESA WorldCover | 10 m | 2020-2021 | Permanent water bodies; herbaceous wetland; mangroves | Sentinel-1 & Sentinel-2 | Zanaga et al. (2021); https://esa-worldcover.org |
| Esri Global Land Cover | 10 m | 2017-2022 | Water; flooded vegetation | Sentinel-2 | Karra et al. (2021); https://livingatlas.arcgis.com/landcover |
| Dynamic World | 10 m | 2015-2023 | Water; flooded vegetation | Sentinel-2 | Brown et al. (2022); https://dynamicworld.app/ |

969

970

971

972 **Table B2~~1~~.** Descriptive characteristics of the 21 verification basins located throughout the CONUS (see Fig. 2).

973 Majority Köppen-Geiger classification follows Beck et al. (2018). Climatological data were acquired from the

974 PRISM Climate Group (Parameter-elevation Regressions on Independent Slopes Model, prism.oregonstate.edu/,

975 accessed 09/26/2022) using the 30-year annual normals for each watershed. Land use data and descriptions are from

976 the 2019 NLCD (www.mrlc.gov/data, accessed 09/26/2022) and represent the land use class with the greatest areal

977 abundance. Average elevation was derived from the USGS National Elevation Dataset (https://www.usgs.gov/3d-

978 elevation-program, accessed 01/13/2022). Global Wetland Count are the counts of wetlands from the derived Global

979 Wetland database within each watershed after region-grouping the data using a four-direction contagion criterion

980 (i.e., pixels immediately adjacent in any of the four cardinal directions are considered part of a unique, multi-pixel

981 wetland, ArcGIS Pro v.2.9.1, Redlands, California).

| Hydrologic Unit Code ID | Area (km$^2$) | Köppen-Geiger | Mean Annual Temp ($^o$C) | Mean Annual Rainfall (m) |
|---|---|---|---|---|
| HUC_0101 | 18,906 | Dfb | 4.0 | 1.1 |
| HUC_0103 | 15,287 | Dfb | 5.4 | 1.2 |
| HUC_0106 | 10,800 | Dfb | 7.5 | 1.3 |
| HUC_0203 | 12,490 | Dfa | 11.6 | 1.2 |
| HUC_0208 | 47,449 | Cfa | 13.7 | 1.2 |
| HUC_0304 | 47,899 | Cfa | 16.4 | 1.3 |
| HUC_0313 | 52,169 | Cfa | 18.1 | 1.4 |
| HUC_0501 | 30,371 | Dfb | 8.6 | 1.2 |
| HUC_0706 | 22,257 | Dfa | 8.1 | 1.0 |
| HUC_0804 | 53,108 | Cfa | 17.5 | 1.4 |
| HUC_1003 | 51,431 | BSk | 5.6 | 0.4 |
| HUC_1015 | 37,098 | Dfa | 8.7 | 0.5 |
| HUC_1016 | 54,743 | Dfa | 6.4 | 0.6 |
| HUC_1024 | 35,237 | Dfa | 10.8 | 0.9 |
| HUC_1029 | 48,204 | Dfa | 13.2 | 1.1 |
| HUC_1304 | 48,126 | BSh | 18.6 | 0.4 |
| HUC_1601 | 19,463 | BSk | 5.7 | 0.5 |
| HUC_1708 | 16,101 | Csb | 9.0 | 2.1 |
| HUC_1711 | 35,651 | Csb | 8.2 | 2.0 |
| HUC_1805 | 11,341 | Csb | 14.9 | 0.7 |
| HUC_1808 | 11,789 | BSk | 8.4 | 0.4 |

982 † Köppen-Geiger Class Descriptions (Beck et al. 2018): BSh (arid, steppe, hot), BSk (arid, steppe, cold), Cfa

983 (temperate, no dry season, hot summer), Csb, (temperature, dry season, warm summer), Dfa (cold, no dry season,

984 hot summer), Dfb (cold, no dry season, warm summer)

985

986 **Table B1B2.** (Continued)

| Hydrologic Unit Code | Majority Land Use Coverage | Majority Land Coverage Description | Global Wetland Count | Average Elevation |
|---|---|---|---|---|
| **HUC_0101** | 43 | Mixed Forest | 2,141 | 296 |
| **HUC_0103** | 43 | Mixed Forest | 2,202 | 300 |
| **HUC_0106** | 43 | Mixed Forest | 2,799 | 169 |
| **HUC_0203** | 41 | Deciduous Forest | 2,438 | 82 |
| **HUC_0208** | 41 | Deciduous Forest | 13,934 | 187 |
| **HUC_0304** | 90 | Woody Wetlands | 14,643 | 127 |
| **HUC_0313** | 42 | Evergreen Forest | 27,056 | 147 |
| **HUC_0501** | 41 | Deciduous Forest | 6,310 | 484 |
| **HUC_0706** | 82 | Cultivated Crops | 3,100 | 300 |
| **HUC_0804** | 42 | Evergreen Forest | 12,242 | 85 |
| **HUC_1003** | 71 | Herbaceous | 11,852 | 1349 |
| **HUC_1015** | 71 | Herbaceous | 8,628 | 961 |
| **HUC_1016** | 82 | Cultivated Crops | 61,482 | 464 |
| **HUC_1024** | 82 | Cultivated Crops | 11,995 | 341 |
| **HUC_1029** | 81 | Hay/Pasture | 23,935 | 297 |
| **HUC_1304** | 52 | Shrub/Scrub | 1,733 | 995 |
| **HUC_1601** | 52 | Shrub/Scrub | 2,642 | 1981 |
| **HUC_1708** | 42 | Evergreen Forest | 1,986 | 552 |
| **HUC_1711** | 42 | Evergreen Forest | 6,562 | 621 |
| **HUC_1805** | 52 | Shrub/Scrub | 1,208 | 222 |
| **HUC_1808** | 52 | Shrub/Scrub | 1,089 | 1625 |

987

988

989 **Table B23.** Floodplain performance assessment of the GFPlain90-derived floodplain and the benchmark floodplain

990 from Woznicki et al. (2019). The first six equations directly assess the spatial concordance and overlap between the

991 two datasets, whereas Mean Absolute Error (Eq. 7) and Aggregate Error Bias (Eq. 8) are coarser fractional analyses

992 (i.e., the fraction of a 1 km$^2$ cell predicted correctly) as measured along the riverine network.

| Hydrologic Unit Code (HUC) ID | Hit Rate (Eq. 1) | Precision (Eq. 2) | False Alarm (Eq. 3) | CSI (Eq. 4) | F1 (Eq. 5) | Error Bias (Eq. 6) | Mean Absolute Error (Eq. 7) | Aggregate Error Bias (Eq. 8) |
|---|---|---|---|---|---|---|---|---|
| HUC_0101 | 0.76 | 0.84 | 0.16 | 0.66 | 0.80 | 0.62 | 0.06 | -0.01 |
| HUC_0103 | 0.92 | 0.77 | 0.23 | 0.72 | 0.84 | 3.25 | 0.05 | 0.03 |
| HUC_0106 | 0.78 | 0.74 | 0.26 | 0.62 | 0.76 | 1.24 | 0.10 | -0.03 |
| HUC_0203 | 0.47 | 0.58 | 0.42 | 0.35 | 0.52 | 0.66 | 0.25 | -0.18 |
| HUC_0208 | 0.64 | 0.73 | 0.27 | 0.52 | 0.68 | 0.67 | 0.13 | -0.08 |
| HUC_0304 | 0.63 | 0.81 | 0.19 | 0.55 | 0.71 | 0.41 | 0.06 | 0.00 |
| HUC_0313 | 0.62 | 0.72 | 0.28 | 0.50 | 0.67 | 0.62 | 0.09 | -0.01 |
| HUC_0501 | 0.77 | 0.85 | 0.15 | 0.68 | 0.81 | 0.59 | 0.04 | -0.02 |
| HUC_0706 | 0.86 | 0.79 | 0.21 | 0.69 | 0.82 | 1.62 | 0.04 | 0.02 |
| HUC_0804 | 0.75 | 0.83 | 0.17 | 0.65 | 0.79 | 0.64 | 0.08 | -0.02 |
| HUC_1003 | 0.85 | 0.42 | 0.58 | 0.39 | 0.56 | 7.70 | 0.11 | 0.09 |
| HUC_1015 | 0.81 | 0.74 | 0.26 | 0.63 | 0.78 | 1.54 | 0.06 | 0.02 |
| HUC_1016 | 0.89 | 0.36 | 0.64 | 0.35 | 0.52 | 14.79 | 0.18 | 0.17 |
| HUC_1024 | 0.90 | 0.88 | 0.12 | 0.80 | 0.89 | 1.19 | 0.03 | 0.00 |
| HUC_1029 | 0.84 | 0.87 | 0.13 | 0.75 | 0.85 | 0.82 | 0.04 | -0.01 |
| HUC_1304 | 0.66 | 0.74 | 0.26 | 0.53 | 0.70 | 0.67 | 0.07 | -0.01 |
| HUC_1601 | 0.92 | 0.55 | 0.45 | 0.52 | 0.69 | 9.47 | 0.10 | 0.08 |
| HUC_1708 | 0.60 | 0.71 | 0.29 | 0.48 | 0.65 | 0.60 | 0.08 | -0.03 |
| HUC_1711 | 0.70 | 0.50 | 0.50 | 0.41 | 0.58 | 2.25 | 0.10 | -0.02 |
| HUC_1805 | 0.59 | 0.59 | 0.41 | 0.41 | 0.59 | 1.00 | 0.14 | -0.05 |
| HUC_1808 | 0.98 | 0.44 | 0.56 | 0.44 | 0.61 | 82.97 | 0.24 | 0.23 |
| Median | 0.77 | 0.74 | 0.26 | 0.53 | 0.70 | 1.00 | 0.08 | -0.01 |
| Mean | 0.76 | 0.69 | 0.31 | 0.56 | 0.71 | 6.35 | 0.10 | 0.01 |

993

994

995
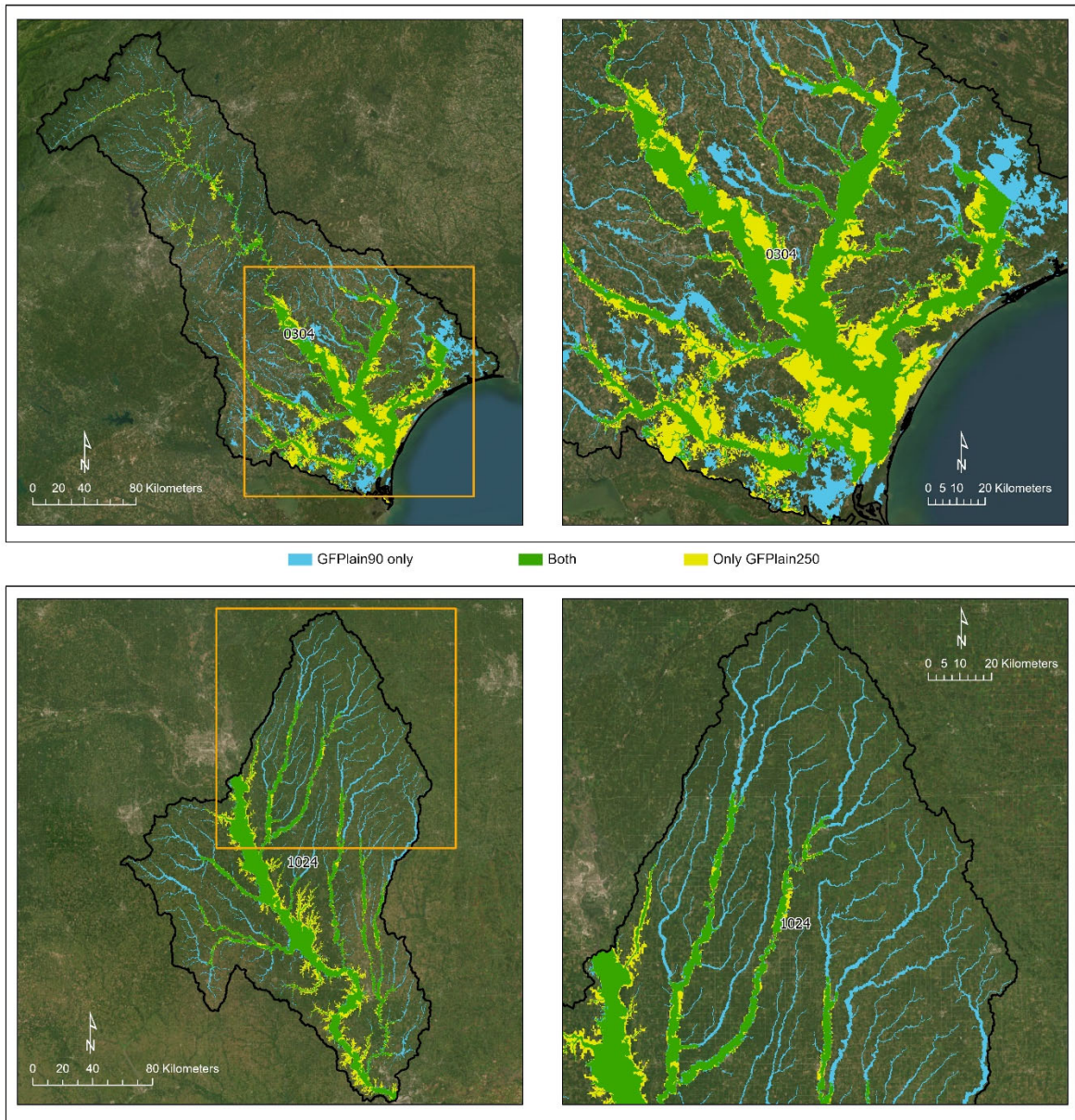
**Figure B1.** Comparison of floodplain extents derived from GFPlain90 (this study) and GFPlain250 (Nardi et al.,
2019). The right-hand panels are the inset area outlined in the orange box on the left panels; the top panels represent
an eastern coastal watershed (HUC_0304) whereas the bottom panels are from a midwestern US watershed
(HUC_1024). The full extent of the riverine network is evident in the GFPlain90 dataset, which was derived from 90
m resolution DEMs in contrast to the 250 m pixel size of the GFPlain250. Satellite imagery sourced from ESRI
(2022).

**References**

Adame, M. F., Arthington, A. H., Waltham, N., Hasan, S., Selles, A., and Ronan, M.: Managing threats and restoring wetlands within catchments of the Great Barrier Reef, Australia, Aquatic Conservation: Marine and Freshwater Ecosystems, 29, 829-839, https://doi.org/10.1002/aqc.3096, 2019.

Alfieri, L., Salamon, P., Bianchi, A., Neal, J., Bates, P., and Feyen, L.: Advances in pan-European flood hazard mapping, Hydrological Processes, 28, 4067-4077, 10.1002/hyp.9947, 2014.

Ameli, A. A. and Creed, I. F.: Does Wetland Location Matter When Managing Wetlands for Watershed-Scale Flood and Drought Resilience?, JAWRA Journal of the American Water Resources Association, 55, 529-542, 10.1111/1752-1688.12737, 2019.

Aronica, G., Bates, P. D., and Horritt, M. S.: Assessing the uncertainty in distributed model predictions using observed binary pattern information within GLUE, Hydrological Processes, 16, 2001-2016, https://doi.org/10.1002/hyp.398, 2002.

Assessment, M. E.: Ecosystems and Human Well-Being: Wetlands and Water Synthesis, World Resources Institute, Washington, D.C., 2005.

Badiou, P., Page, B., and Akinremi, W.: Phosphorus Retention in Intact and Drained Prairie Wetland Basins: Implications for Nutrient Export, Journal of Environmental Quality, 47, 902-913, https://doi.org/10.2134/jeq2017.08.0336, 2018.

Bam, E. K. P., Ireson, A. M., van der Kamp, G., and Hendry, J. M.: Ephemeral Ponds: Are They the Dominant Source of Depression-Focused Groundwater Recharge?, Water Resources Research, 56, e2019WR026640, https://doi.org/10.1029/2019WR026640, 2020.

Bates, P. D. and De Roo, A. P. J.: A simple raster-based model for flood inundation simulation, Journal of Hydrology, 236, 54-77, http://dx.doi.org/10.1016/S0022-1694(00)00278-X, 2000.

Beck, H. E., Zimmermann, N. E., McVicar, T. R., Vergopolan, N., Berg, A., and Wood, E. F.: Present and future Köppen-Geiger climate classification maps at 1-km resolution, Scientific Data, 5, 180214, 10.1038/sdata.2018.214, 2018.

1028 Berhane, T., Lane, C., Wu, Q., Autrey, B., Anenkhonov, O., Chepinoga, V., and Liu, H.: Decision-Tree,

1029      Rule-Based, and Random Forest Classification of High-Resolution Multispectral Imagery for Wetland

1030      Mapping and Inventory, Remote Sensing, 10, 580, 2018.

1031 Biggs, J., von Fumetti, S., and Kelly-Quinn, M.: The importance of small waterbodies for biodiversity

1032      and ecosystem services: implications for policy makers, Hydrobiologia, 793, 3-39, 10.1007/s10750-

1033      016-3007-0, 2017.

1034 Blanchette, M., Rousseau, A. N., Savary, S., and Foulon, É.: Are spatial distribution and aggregation of

1035      wetlands reliable indicators of stream flow mitigation?, Journal of Hydrology, 608, 127646,

1036      https://doi.org/10.1016/j.jhydrol.2022.127646, 2022.

1037 Brown, C. F., Brumby, S. P., Guzder-Williams, B., Birch, T., Hyde, S. B., Mazzariello, J., Czerwinski,

1038      W., Pasquarella, V. J., Haertel, R., Ilyushchenko, S., Schwehr, K., Weisse, M., Stolle, F., Hanson, C.,

1039      Guinan, O., Moore, R., and Tait, A. M.: Dynamic World, Near real-time global 10 m land use land

1040      cover mapping, Scientific Data, 9, 251, 10.1038/s41597-022-01307-4, 2022.

1041 Buttle, J. M.: Mediating stream baseflow response to climate change: The role of basin storage,

1042      Hydrological Processes, 32, 363-378, 10.1002/hyp.11418, 2018.

1043 Chen, J., Chen, J., Liao, A., Cao, X., Chen, L., Chen, X., He, C., Han, G., Peng, S., Lu, M., Zhang, W.,

1044      Tong, X., and Mills, J.: Global land cover mapping at 30m resolution: A POK-based operational

1045      approach, ISPRS Journal of Photogrammetry and Remote Sensing, 103, 7-27,

1046      https://doi.org/10.1016/j.isprsjprs.2014.09.002, 2015.

1047 Chen, W., Thorslund, J., Nover, D. M., Rains, M. C., Li, X., Xu, B., He, B., Su, H., Yen, H., Liu, L.,

1048      Yuan, H., Jarsjö, J., and Viers, J. H.: A typological framework of non-floodplain wetlands for global

1049      collaborative research and sustainable use, Environmental Research Letters, 17, 113002, 10.1088/1748-

1050      9326/ac9850, 2022.

1051 Cheng, F. Y. and Basu, N. B.: Biogeochemical hotspots: Role of small water bodies in landscape nutrient

1052      processing, Water Resources Research, 53, 5038-5056, 10.1002/2016WR020102, 2017.

1053    Cheng, F. Y., Van Meter, K. J., Byrnes, D. K., and Basu, N. B.: Maximizing US nitrate removal through

1054        wetland protection and restoration, Nature, 588, 625-630, 10.1038/s41586-020-03042-5, 2020.

1055    Christensen, J. R., Golden, H. E., Alexander, L. C., Pickard, B. R., Fritz, K. M., Lane, C. R., Weber, M.

1056        H., Kwok, R. M., and Keefer, M. N.: Headwater streams and inland wetlands: Status and advancements

1057        of geospatial datasets and maps across the United States, Earth-Science Reviews, 104230,

1058        https://doi.org/10.1016/j.earscirev.2022.104230, 2022.

1059    Cohen, M. J., Creed, I. F., Alexander, L., Basu, N. B., Calhoun, A. J. K., Craft, C., D'Amico, E.,

1060        DeKeyser, E., Fowler, L., Golden, H. E., Jawitz, J. W., Kalla, P., Kirkman, L. K., Lane, C. R., Lang,

1061        M., Leibowitz, S. G., Lewis, D. B., Marton, J., McLaughlin, D. L., Mushet, D. M., Raanan-Kiperwas,

1062        H., Rains, M. C., Smith, L., and Walls, S. C.: Do geographically isolated wetlands influence landscape

1063        functions?, Proceedings of the National Academy of Sciences, 113, 1978-1986,

1064        10.1073/pnas.1512650113, 2016.

1065    Colvin, S. A. R., Sullivan, S. M. P., Shirey, P. D., Colvin, R. W., Winemiller, K. O., Hughes, R. M.,

1066        Fausch, K. D., Infante, D. M., Olden, J. D., Bestgen, K. R., Danehy, R. J., and Eby, L.: Headwater

1067        Streams and Wetlands are Critical for Sustaining Fish, Fisheries, and Ecosystem Services, Fisheries, 44,

1068        73-91, 2019.

1069    Cowardin, L. M., Carter, V., Golet, F. C., and LaRoe, E. T.: Classification of Wetlands and Deepwater

1070        habitats of The United States, Fish and Wildlife Service, Washington DCFWS/OBS-79/31, 1979.

1071    Creed, I. F., Lane, C. R., Serran, J. N., Alexander, L. C., Basu, N. B., Calhoun, A. J. K., Christensen, J.

1072        R., Cohen, M. J., Craft, C., D'Amico, E., DeKeyser, E., Fowler, L., Golden, H. E., Jawitz, J. W., Kalla,

1073        P., Kirkman, L. K., Lang, M., Leibowitz, S. G., Lewis, D. B., Marton, J., McLaughlin, D. L., Raanan-

1074        Kiperwas, H., Rains, M. C., Rains, K. C., and Smith, L.: Enhancing protection for vulnerable waters,

1075        Nature Geoscience, 10, 809-815, 10.1038/ngeo3041, 2017.

1076    Cunha, D. G. F., Magri, R. A. F., Tromboni, F., Ranieri, V. E. L., Fendrich, A. N., Campanhão, L. M. B.,

1077        Riveros, E. V., and Velázquez, J. A.: Landscape patterns influence nutrient concentrations in aquatic

1078    systems: citizen science data from Brazil and Mexico, Freshwater Science, 38, 365-378,

1079    10.1086/703396, 2019.

1080  Dahl, T. E.: Wetlands - Losses in the United States, 1780's to 1980's, U.S. Department of Interior, Fish

1081    and Wildlife Service Washington DC, 1990.

1082  Davidson, N. C.: How much wetland has the world lost? Long-term and recent trends in global wetland

1083    area, Marine and Freshwater Research, 65, 934-941, http://dx.doi.org/10.1071/MF14173, 2014.

1084  Davidson, N. C., E. Fluet-Chouinard and C. M. Finlayson. 2018. Global extent and distribution of

1085    wetlands: trends and issues. Marine and Freshwater Research 69, 4, 620-627, 2018.

1086  De Groot, R., M. Stuip, M. Finlayson, and N. Davidson: Valuing Wetlands: Guidance for Valuing the

1087    Benefits Derived from Wetland Ecosystem Services, Ramsar Convention Secretariat, Gland,

1088    Switzerland and Secretariat of the Convention on Biological Diversity, Montreal, Canada, Gland,

1089    SwitzerlandRamsar Technical Report No. 3/CBD Technical Series No. 27, 2006.

1090  DeVries, B., Huang, C., Lang, M., Jones, J., Huang, W., Creed, I., and Carroll, M.: Automated

1091    Quantification of Surface Water Inundation in Wetlands Using Optical Satellite Imagery, Remote

1092    Sensing, 9, 807, 2017.

1093  Dewitz, J.: National Land Cover Database (NLCD) 2016 Products: U.S. Geological Survey data release

1094    [dataset], https://doi.org/10.5066/P96HHBIE, 2019.

1095  Drenkhan, F., Buytaert, W., Mackay, J. D., Barrand, N. E., Hannah, D. M., and Huggel, C.: Looking

1096    beyond glaciers to understand mountain water security, Nature Sustainability, 10.1038/s41893-022-

1097    00996-4, 2022.

1098  ESA Worldwide Land Cover Mapping: https://esa-worldcover.org/en, last access: 22 Deccember 2022.

1099  ESA Land Cover CCI, Product User Guide Version 2.0:

1100    https://maps.elie.ucl.ac.be/CCI/viewer/download/ESACCI-LC-Ph2-PUGv2_2.0.pdf, last access: May

1101    2022.

1102 ESRI World Terrain Base

1103 https://www.arcgis.com/home/item.html?id=be2e229ffc864c868a78f5ca68ca5b8e, last accessed 22

1104 December 2022.

1105 Evenson, G. R., Golden, H. E., Lane, C. R., McLaughlin, D. L., and D'Amico, E.: Depressional Wetlands

1106 Affect Watershed Hydrological, Biogeochemical, and Ecological Functions, Ecological Applications,

1107 28, 953-966, 10.1002/eap.1701, 2018a.

1108 Evenson, G. R., Jones, C. N., McLaughlin, D. L., Golden, H. E., Lane, C. R., DeVries, B., Alexander, L.

1109 C., Lang, M. W., McCarty, G. W., and Sharifi, A.: A watershed-scale model for depressional wetland-

1110 rich landscapes, Journal of Hydrology X, 1, 100002, https://doi.org/10.1016/j.hydroa.2018.10.002,

1111 2018b.

1112 Evenson, G. R., Golden, H. E., Christensen, J. R., Lane, C. R., Rajib, A., D'Amico, E., Mahoney, D. T.,

1113 White, E., and Wu, Q.: Wetland restoration yields dynamic nitrate responses across the Upper

1114 Mississippi river basin, Environmental Research Communications, 3, 095002, 10.1088/2515-

1115 7620/ac2125, 2021.

1116 Fan, Y., Li, H., and Miguez-Macho, G.: Global Patterns of Groundwater Table Depth, Science, 339, 940-

1117 943, doi:10.1126/science.1229881, 2013.

1118 Fewtrell, T. J., Bates, P. D., Horritt, M., and Hunter, N. M.: Evaluating the effect of scale in flood

1119 inundation modelling in urban environments, Hydrological Processes, 22, 5107-5118,

1120 https://doi.org/10.1002/hyp.7148, 2008.

1121 Fluet-Chouinard, E., Lehner, B., Rebelo, L.-M., Papa, F., and Hamilton, S. K.: Development of a global

1122 inundation map at high spatial resolution from topographic downscaling of coarse-scale remote sensing

1123 data, Remote Sensing of Environment, 158, 348-361, https://doi.org/10.1016/j.rse.2014.10.015, 2015.

1124 Fluet-Chouinard, E., B. D. Stocker, Z. Zhang, A. Malhotra, J. R. Melton, B. Poulter, J. O. Kaplan, K. K.

1125 Goldewijk, S. Siebert, T. Minayeva, G. Hugelius, H. Joosten, A. Barthelmes, C. Prigent, F. Aires, A. M.

1126 Hoyt, N. Davidson, C. M. Finlayson, B. Lehner, R. B. Jackson and P. B. McIntyre. Extensive global

1127 wetland loss over the past three centuries, Nature, 614, 7947, 281-286, 2023.

Fossey, M. and Rousseau, A. N.: Can isolated and riparian wetlands mitigate the impact of climate change on watershed hydrology? A case study approach, Journal of Environmental Management, 184(2):327-339, http://dx.doi.org/10.1016/j.jenvman.2016.09.043, 2016.

Golden, H. E., Lane, C. R., Rajib, A., and Wu, Q.: Improving global flood and drought predictions: integrating non-floodplain wetlands into watershed hydrologic models, Environmental Research Letters, 16, 091002, 10.1088/1748-9326/ac1fbc, 2021.

Golden, H. E., Rajib, A., Lane, C. R., Christensen, J. R., Wu, Q., and Mengistu, S.: Non-floodplain Wetlands Affect Watershed Nutrient Dynamics: A Critical Review, Environmental Science & Technology, 53, 7203-7214, 10.1021/acs.est.8b07270, 2019.

Golden, H. E., Sander, H. A., Lane, C. R., Zhao, C., Price, K., D'Amico, E., and Christensen, J. R.: Relative effects of geographically isolated wetlands on streamflow: a watershed-scale analysis, Ecohydrology, 9, 21-38, 10.1002/eco.1608, 2016.

Golden, H. E., Creed, I. F., Ali, G., Basu, N. B., Neff, B. P., Rains, M. C., McLaughlin, D. L., Alexander, L. C., Ameli, A. A., Christensen, J. R., Evenson, G. R., Jones, C. N., Lane, C. R., and Lang, M.: Integrating geographically isolated wetlands into land management decisions, Frontiers in Ecology and the Environment, 15, 319-327, 10.1002/fee.1504, 2017.

Gumbricht, T., Roman-Cuesta, R. M., Verchot, L., Herold, M., Wittmann, F., Householder, E., Herold, N., and Murdiyarso, D.: An expert system model for mapping tropical wetlands and peatlands reveals South America as the largest contributor, Global Change Biology, 23, 3581-3599, https://doi.org/10.1111/gcb.13689, 2017.

Hamunyela, E., Hipondoka, M., Persendt, F., Sevelia Nghiyalwa, H., Thomas, C., and Matengu, K.: Spatio-temporal characterization of surface water dynamics with Landsat in endorheic Cuvelai-Etosha Basin (1990–2021), ISPRS Journal of Photogrammetry and Remote Sensing, 191, 68-84, https://doi.org/10.1016/j.isprsjprs.2022.07.007, 2022.

Hoch, J. M. and M. A. Trigg. Advancing global flood hazard simulations by improving comparability, benchmarking, and integration of global flood models. Environmental Research Letters, 14, 3, 034001, 2019.

Homer, C., Dewitz, J., Jin, S., Xian, G., Costello, C., Danielson, P., Gass, L., Funk, M., Wickham, J., Stehman, S., Auch, R., and Riitters, K.: Conterminous United States land cover change patterns 2001–2016 from the 2016 National Land Cover Database, ISPRS Journal of Photogrammetry and Remote Sensing, 162, 184-199, https://doi.org/10.1016/j.isprsjprs.2020.02.019, 2020.

Horritt, M. S. and Bates, P. D.: Evaluation of 1D and 2D numerical models for predicting river flood inundation, Journal of Hydrology, 268, 87-99, http://dx.doi.org/10.1016/S0022-1694(02)00121-X, 2002.

Hu, S., Niu, Z., and Chen, Y.: Global Wetland Datasets: a Review, Wetlands, 37, 807-817, 10.1007/s13157-017-0927-z, 2017a.

Hu, S., Niu, Z., Chen, Y., Li, L., and Zhang, H.: Global wetlands: Potential distribution, wetland loss, and status, Science of The Total Environment, 586, 319-327, http://dx.doi.org/10.1016/j.scitotenv.2017.02.001, 2017b.

Huang, W., DeVries, B., Huang, C., Lang, M., Jones, J., Creed, I., and Carroll, M.: Automated Extraction of Surface Water Extent from Sentinel-1 Data, Remote Sensing, 10, 797, 2018.

IPCC: Intergovernmental Panel on Climate Change 2014: Impacts, adaptation, and vulnerability, Cambridge University Press, Cambridge, U.K.2014.

Jafarzadegan, K., Merwade, V., and Saksena, S.: A geomorphic approach to 100-year floodplain mapping for the Conterminous United States, Journal of Hydrology, 561, 43-58, https://doi.org/10.1016/j.jhydrol.2018.03.061, 2018.

Jakubínský, J., Prokopová, M., Raška, P., Salvati, L., Bezak, N., Cudlín, O., Cudlín, P., Purkyt, J., Vezza, P., Camporeale, C., Daněk, J., Pástor, M., and Lepeška, T.: Managing floodplains using nature-based solutions to support multiple ecosystem functions and services, WIREs Water, 8, e1545, https://doi.org/10.1002/wat2.1545, 2021.

Jin, S., Homer, C., Yang, L., Danielson, P., Dewitz, J., Li, C., Zhu, Z., Xian, G., and Howard, D.: Overall Methodology Design for the United States National Land Cover Database 2016 Products, Remote Sensing, 11, 2971, 2019.

Jones, C. N., Evenson, G. R., McLaughlin, D. L., Vanderhoof, M. K., Lang, M. W., McCarty, G. W., Golden, H. E., Lane, C. R., and Alexander, L. C.: Estimating restorable wetland water storage at landscape scales, Hydrological Processes, 32, 305-313, 10.1002/hyp.11405, 2018.

Karra, K., Kontgis, C., Statman-Weil, Z., Mazzariello, J. C., Mathis, M., & Brumby, S. P. Global land use/land cover with Sentinel 2 and deep learning. In: 2021 IEEE International Geoscience and Remote Sensing Symposium IGARSS (pp. 4704-4707). IEEE, doi.org/10.1109/IGARSS47720.2021.9553499, 2021.

Kam, S. P.: Valuing the role of living aquatic resources to rural livelihoods in multiple-use, seasonally-inundated wetlands in the Yellow River Basin of China, for improved governance, CGIAR Challenge Program on Water & Food, Colombo, Sri Lanka, https://hdl.handle.net/10568/3859, 2010.

Khare, A., Rajib, A., Zheng, Q., Golden, H. E., Wu, Q., Lane, C. R., Christensen, J. R., Dahl, T. A., Ryder, J. L., and McFall, B. C.: Global surface water estimates: Critical need for data consistency and integration, Nature Water, in review.

Kremenetski, K. V., Velichko, A. A., Borisova, O. K., MacDonald, G. M., Smith, L. C., Frey, K. E., and Orlova, L. A.: Peatlands of the Western Siberian lowlands: current knowledge on zonation, carbon content and Late Quaternary history, Quaternary Science Reviews, 22, 703-723, 2003.

Kundzewicz, Z. W., Hegger, D. L. T., Matczak, P., and Driessen, P. P. J.: Opinion: Flood-risk reduction: Structural measures and diverse strategies, Proceedings of the National Academy of Sciences, 115, 12321-12325, 10.1073/pnas.1818227115, 2018.

Lane, C. R. and D'Amico, E.: Identification of Putative Geographically Isolated Wetlands of the Conterminous United States, JAWRA Journal of the American Water Resources Association, 52, 705-722, 10.1111/1752-1688.12421, 2016.

Lane, C. R., Leibowitz, S. G., Autrey, B. C., LeDuc, S. D., and Alexander, L. C.: Hydrological, Physical, and Chemical Functions and Connectivity of Non-Floodplain Wetlands to Downstream Waters: A Review, JAWRA Journal of the American Water Resources Association, 54, 346-371, 10.1111/1752-1688.12633, 2018.

Lane, C. R., Creed, I. F., Golden, H. E., Leibowitz, S. G., Mushet, D. M., Rains, M. C., Wu, Q., D'Amico, E., Alexander, L. C., Ali, G. A., Basu, N. B., Bennett, M. G., Christensen, J. R., Cohen, M. J., Covino, T. P., DeVries, B., Hill, R. A., Jencso, K., Lang, M. W., McLaughlin, D. L., Rosenberry, D. O., Rover, J., and Vanderhoof, M. K.: Vulnerable Waters are Essential to Watershed Resilience, Ecosystems, 10.1007/s10021-021-00737-2, 2022.

Lane, C. R., E. D'Amico, J. R. Christensen, H. E. Golden, Q. Wu, and A. Rajib. Global non-floodplain wetlands [dataset], https://gaftp.epa.gov/EPADataCommons/ORD/Global_NonFloodplain_Wetlands/ and https://doi.org/10.23719/1528331, 2023.

Lehner, B. and Doll, P.: Development and validation of a global database of lakes, reservoirs and wetlands, Journal of Hydrology, 296, 1-22, 2004.

Lehner, B. and Grill, G.: Global river hydrography and network routing: baseline data and new approaches to study the world's large river systems, Hydrological Processes, 27, 2171-2186, https://doi.org/10.1002/hyp.9740, 2013.

Leibowitz, S.: Geographically Isolated Wetlands: Why We Should Keep the Term, Wetlands, 35, 997-1003, 10.1007/s13157-015-0691-x, 2015.

Leibowitz, S. G.: Isolated wetlands and their functions: an ecological perspective, Wetlands, 22, 517-531, 2003.

Leibowitz, S. G., Hill, R. A., Creed, I. F., Compton, J. E., Golden, H. E., Weber, M. H., Rains, M. C., Jones, J., C. E., Lee, E. H., Christensen, J. R., Bellmore, R. A., and Lane, C. R.: National hydrologic connectivity classification links wetlands with stream water qualityConnections matter: National classification links wetlands and water quality, ScienceNature Water, In Review1, 370-380, DOI: 10.1038/s44221-023-00057-w, 2023.

1229     Liu, D., Cao, C., Chen, W., Ni, X., Tian, R., and Xing, X.: Monitoring and predicting the degradation of a

1230        semi-arid wetland due to climate change and water abstraction in the Ordos Larus relictus National

1231        Nature Reserve, China, Geomatics, Natural Hazards and Risk, 8, 367-383,

1232        10.1080/19475705.2016.1220024, 2017.

1233     Makungu, E. and Hughes, D. A.: Understanding and modelling the effects of wetland on the hydrology

1234        and water resources of large African river basins, Journal of Hydrology, 603, 127039,

1235        https://doi.org/10.1016/j.jhydrol.2021.127039, 2021.

1236     Martinis, S., Groth, S., Wieland, M., Knopp, L., and Rättich, M.: Towards a global seasonal and

1237        permanent reference water product from Sentinel-1/2 data for improved flood mapping, Remote

1238        Sensing of Environment, 278, 113077, https://doi.org/10.1016/j.rse.2022.113077, 2022.

1239     Marton, J. M., Creed, I. F., Lewis, D., Lane, C. R., Basu, N., Cohen, M. J., and C., C.: Geographically

1240        isolated wetlands are important biogeochemical reactors on the landscape, BioScience, 65, 408-418,

1241        10.1093/biosci/biv009, 2015.

1242     McCauley, L. A., Anteau, M. J., van der Burg, M. P., and Wiltermuth, M. T.: Land use and wetland

1243        drainage affect water levels and dynamics of remaining wetlands, Ecosphere, 6, art92, 10.1890/ES14-

1244        00494.1, 2015.

1245     McKenna, O. P., Mushet, D. M., Rosenberry, D. O., and LaBaugh, J. W.: Evidence for a climate-induced

1246        ecohydrological state shift in wetland ecosystems of the southern Prairie Pothole Region, Climatic

1247        Change, 145, 273-287, 10.1007/s10584-017-2097-7, 2017.

1248     McLaughlin, D. L., Kaplan;, D. A., and Cohen, M. J.: A significant nexus: Geographically isolated

1249        wetlands influence landscape hydrology, Water Resources Research, 50, 7153-7166,

1250        10.1002/2013WR015002, 2014.

1251     Merken, R., Deboelpaep, E., Teunen, J., Saura, S., and Koedam, N.: Wetland Suitability and Connectivity

1252        for Trans-Saharan Migratory Waterbirds, PLOS ONE, 10, e0135445, 10.1371/journal.pone.0135445,

1253        2015.

Messager, M. L., Lehner, B., Grill, G., Nedeva, I., and Schmitt, O.: Estimating the volume and age of water stored in global lakes using a geo-statistical approach, Nature Communications, 7, 13603, 10.1038/ncomms13603, 2016.

Mudashiru, R. B., N. Sabtu, I. Abustan and W. Balogun. Flood hazard mapping methods: A review. Journal of Hydrology, 603, 126846, 2021.

Mushet, D., Calhoun, A., Alexander, L., Cohen, M., DeKeyser, E., Fowler, L., Lane, C., Lang, M., Rains, M., and Walls, S.: Geographically Isolated Wetlands: Rethinking a Misnomer, Wetlands, 35, 423-431, 10.1007/s13157-015-0631-9, 2015.

Mushet, D. M., Alexander, L. C., Bennett, M., Schofield, K., Christensen, J. R., Ali, G., Pollard, A., Fritz, K., and Lang, M. W.: Differing Modes of Biotic Connectivity within Freshwater Ecosystem Mosaics, JAWRA Journal of the American Water Resources Association, 55, 307-317, 10.1111/1752-1688.12683, 2019.

Nardi, F., Annis, A., Di Baldassarre, G., Vivoni, E. R., and Grimaldi, S.: GFPLAIN250m, a global high-resolution dataset of Earth's floodplains, Scientific Data, 6, 180309, 10.1038/sdata.2018.309, 2019.

National Landcover Database (NLCD) 2019 NLCD Land Cover (CONUS), https://www.mrlc.gov/data, last accessed 22 December 2022.

Nitzsche, K. N., Kalettka, T., Premke, K., Lischeid, G., Gessler, A., and Kayler, Z. E.: Land-use and hydroperiod affect kettle hole sediment carbon and nitrogen biogeochemistry, Science of The Total Environment, 574, 46-56, http://dx.doi.org/10.1016/j.scitotenv.2016.09.003, 2017.

Olefeldt, D., Hovemyr, M., Kuhn, M. A., Bastviken, D., Bohn, T. J., Connolly, J., Crill, P., Euskirchen, E. S., Finkelstein, S. A., Genet, H., Grosse, G., Harris, L. I., Heffernan, L., Helbig, M., Hugelius, G., Hutchins, R., Juutinen, S., Lara, M. J., Malhotra, A., Manies, K., McGuire, A. D., Natali, S. M., O'Donnell, J. A., Parmentier, F. J. W., Räsänen, A., Schädel, C., Sonnentag, O., Strack, M., Tank, S. E., Treat, C., Varner, R. K., Virtanen, T., Warren, R. K., and Watts, J. D.: The Boreal–Arctic Wetland and Lake Dataset (BAWLD), Earth Syst. Sci. Data, 13, 5127-5149, 10.5194/essd-13-5127-2021, 2021.

Pappenberger, F., E. Dutra, F. Wetterhall and H. L. Cloke. Deriving global flood hazard maps of fluvial

    floods through a physical model cascade. Hydrol. Earth Syst. Sci., 16, 11, 4143-4156, 2012.

Pekel, J.-F., Cottam, A., Gorelick, N., and Belward, A. S.: High-resolution mapping of global surface

    water and its long-term changes, Nature, 540, 418-422, 10.1038/nature20584, 2016.

Prigent, C., Papa, F., Aires, F., Rossow, W. B., and Matthews, E.: Global inundation dynamics inferred

    from multiple satellite observations, 1993–2000, Journal of Geophysical Research: Atmospheres, 112,

    https://doi.org/10.1029/2006JD007847, 2007.

PRISM Climate Group, Parameter-elevation Regressions on Independent Slopes Model,

    prism.oregonstate.edu/, last accessed 22 December 2022.

Rains, M. C., Leibowitz, S. G., Cohen, M. J., Creed, I. F., Golden, H. E., Jawitz, J. W., Kalla, P., Lane, C.

    R., Lang, M. W., and McLaughlin, D. L.: Geographically isolated wetlands are part of the hydrological

    landscape, Hydrological Processes, 30, 153-160, 10.1002/hyp.10610, 2016.

Rajib, A., Golden, H. E., Lane, C. R., and Wu, Q.: Surface depression and wetland water storage

    improves major river basin hydrologic predictions, Water Resources Research, 56, e2019WR026561,

    https://doi.org/10.1029/2019WR026561, 2020.

Rajib, A., Zheng, Q., Lane, C. R., Golden, H. E., Christensen, J. R., Isibor, I., and Johnson, K.: Human

    alterations of the world's floodplains Scientific Data, in review.

Rajib, A., Zheng, Q., Golden, H. E., Wu, Q., Lane, C. R., Christensen, J. R., Morrison, R. R., Annis, A.,

    and Nardi, F.: The changing face of floodplains in the Mississippi River Basin detected by a 60-year

    land use change dataset, Scientific Data, 8, 271, 10.1038/s41597-021-01048-w, 2021.

Robarts, R., Zhulidov, A., and Pavlov, D.: The State of knowledge about wetlands and their future under

    aspects of global climate change: the situation in Russia, Aquatic Sciences, 75, 27-38, 10.1007/s00027-

    011-0230-7, 2013.

1302    Rodrigues, L. N., Sano, E. E., Steenhuis, T. S., and Passo, D. P.: Estimation of Small Reservoir Storage

1303        Capacities with Remote Sensing in the Brazilian Savannah Region, Water Resources Management, 26,

1304        873-882, 10.1007/s11269-011-9941-8, 2012.

1305    Rodríguez-Rodríguez, M., Aguilera, H., Guardiola-Albert, C., and Fernández-Ayuso, A.: Climate

1306        Influence Vs. Local Drivers in Surface Water-Groundwater Interactions in Eight Ponds of Doñana

1307        National Park (Southern Spain), Wetlands, 41, 25, 10.1007/s13157-021-01425-6, 2021.

1308    Rudari, R., Silvestro, F., Campo, L., Rebora, N., Boni, G., and Herold, C. Improvement of the global

1309        flood model for the GAR 2015. United Nations Office for Disaster Risk Reduction (UNISDR), Centro

1310        Internazionale in Monitoraggio Ambientale (CIMA), UNEP GRID-Arendal (GRID-Arendal): Geneva,

1311        Switzerland, 69, 2015.

1312    Sampson, C. C., Smith, A. M., Bates, P. D., Neal, J. C., Alfieri, L., and Freer, J. E.: A high-resolution

1313        global flood hazard model, Water Resources Research, 51, 7358-7381, 10.1002/2015WR016954, 2015.

1314    Samways, M. J., Deacon, C., Kietzka, G. J., Pryke, J. S., Vorster, C., and Simaika, J. P.: Value of

1315        artificial ponds for aquatic insects in drought-prone southern Africa: a review, Biodiversity and

1316        Conservation, 29, 3131-3150, 10.1007/s10531-020-02020-7, 2020.

1317    Sangwan, N. and Merwade, V.: A Faster and Economical Approach to Floodplain Mapping Using Soil

1318        Information, JAWRA Journal of the American Water Resources Association, 51, 1286-1304,

1319        10.1111/1752-1688.12306, 2015.

1320    Schofield, K. A., Alexander, L. C., Ridley, C. E., Vanderhoof, M. K., Fritz, K. M., Autrey, B. C.,

1321        DeMeester, J. E., Kepner, W. G., Lane, C. R., Leibowitz, S. G., and Pollard, A. I.: Biota Connect

1322        Aquatic Habitats throughout Freshwater Ecosystem Mosaics, JAWRA Journal of the American Water

1323        Resources Association, 54, 372-399, 10.1111/1752-1688.12634, 2018.

1324    Serran, J. N., Creed, I. F., Ameli, A. A., and Aldred, D. A.: Estimating rates of wetland loss using power-

1325        law functions, Wetlands, 38, 109-120, 10.1007/s13157-017-0960-y, 2017.

1326  Shaw, D. A., Vanderkamp, G., Conly, F. M., Pietroniro, A., and Martz, L.: The Fill–Spill Hydrology of

1327     Prairie Wetland Complexes during Drought and Deluge, Hydrological Processes, 26, 3147-3156,

1328     10.1002/hyp.8390, 2012.

1329  Smith, L. L., Subalusky, A. L., Atkinson, C. L., Earl, J. E., Mushet, D. M., Scott, D. E., Lance, S. L., and

1330     Johnson, S. A.: Biological Connectivity of Seasonally Ponded Wetlands across Spatial and Temporal

1331     Scales, JAWRA Journal of the American Water Resources Association, 55, 334-353, 10.1111/1752-

1332     1688.12682, 2019.

1333  Strahler, A. N.: Quantitative analysis of watershed geomorphology, American Geophysical Union

1334     Transactions, 38, 913-920, 1957.

1335  Sullivan, S. M. P., Rains, M. C., and Rodewald, A. D.: Opinion: The proposed change to the definition of

1336     "waters of the United States" flouts sound science, Proceedings of the National Academy of Sciences,

1337     116, 11558, 10.1073/pnas.1907489116, 2019.

1338  Tayefi, V., Lane, S. N., Hardy, R. J., and Yu, D.: A comparison of one- and two-dimensional approaches

1339     to modelling flood inundation over complex upland floodplains, Hydrological Processes, 21, 3190-

1340     3202, 10.1002/hyp.6523, 2007.

1341  Tootchi, A., Jost, A., and Ducharne, A.: Multi-source global wetland maps combining surface water

1342     imagery and groundwater constraints, Earth Syst. Sci. Data, 11, 189-220, 10.5194/essd-11-189-2019,

1343     2019.

1344  Tsendbazar, N., Herold, M., Li, L., Tarko, A., de Bruin, S., Masiliunas, D., Lesiv, M., Fritz, S., Buchhorn,

1345     M., Smets, B., Van De Kerchove, R., and Duerauer, M.: Towards operational validation of annual

1346     global land cover maps, Remote Sensing of Environment, 266, 112686,

1347     https://doi.org/10.1016/j.rse.2021.112686, 2021.

1348  Tullos, D.: Opinion: How to achieve better flood-risk governance in the United States, Proceedings of the

1349     National Academy of Sciences, 115, 3731-3734, 10.1073/pnas.1722412115, 2018.

Uden, D. R., Allen, C. R., Bishop, A. A., Grosse, R., Jorgensen, C. F., LaGrange, T. G., Stutheit, R. G., and Vrtiska, M. P.: Predictions of future ephemeral springtime waterbird stopover habitat availability under global change, Ecosphere, 6, 1-26, 10.1890/ES15-00256.1, 2015.

United States Geological Survey (USGS) National Elevation Dataset, https://www.usgs.gov/3d-elevation-program, last accessed 22 December 2022.

United States Geological Survey (USGS) Watershed Boundary Dataset, https://www.usgs.gov/national-hydrography/access-national-hydrography-products, last accessed 22 December 2022.

Van Meter, K. J. and Basu, N. B.: Signatures of human impact: size distributions and spatial organization of wetlands in the Prairie Pothole landscape, Ecological Applications, 25, 451-465, 10.1890/14-0662.1, 2015.

Van Meter, K. J., Basu, N. B., Tate, E., and Wyckoff, J.: Monsoon Harvests: The Living Legacies of Rainwater Harvesting Systems in South India, Environmental Science & Technology, 48, 4217-4225, 10.1021/es4040182, 2014.

Vanderhoof, M. K. and Lane, C. R.: The potential role of very high-resolution imagery to characterise lake, wetland and stream systems across the Prairie Pothole Region, United States, International Journal of Remote Sensing, 40, 5768-5798, 10.1080/01431161.2019.1582112, 2019.

Wania, R., Melton, J. R., Hodson, E. L., Poulter, B., Ringeval, B., Spahni, R., Bohn, T., Avis, C. A., Chen, G., Eliseev, A. V., Hopcroft, P. O., Riley, W. J., Subin, Z. M., Tian, H., van Bodegom, P. M., Kleinen, T., Yu, Z. C., Singarayer, J. S., Zürcher, S., Lettenmaier, D. P., Beerling, D. J., Denisov, S. N., Prigent, C., Papa, F., and Kaplan, J. O.: Present state of global wetland extent and wetland methane modelling: methodology of a model inter-comparison project (WETCHIMP), Geosci. Model Dev., 6, 617-641, 10.5194/gmd-6-617-2013, 2013.

Werner, M. G. F., Hunter, N. M., and Bates, P. D.: Identifiability of distributed floodplain roughness values in flood extent estimation, Journal of Hydrology, 314, 139-157, https://doi.org/10.1016/j.jhydrol.2005.03.012, 2005.

Wickham, J., Stehman, S. V., Sorenson, D. G., Gass, L., and Dewitz, J. A.: Thematic accuracy assessment of the NLCD 2016 land cover for the conterminous United States, Remote Sensing of Environment, 257, 112357, https://doi.org/10.1016/j.rse.2021.112357, 2021.

Wing, O. E. J., Bates, P. D., Sampson, C. C., Smith, A. M., Johnson, K. A., and Erickson, T. A.: Validation of a 30 m resolution flood hazard model of the conterminous United States, Water Resources Research, 53, 7968-7986, 10.1002/2017WR020917, 2017.

Winsemius, H. C., L. P. H. Van Beek, B. Jongman, P. J. Ward and A. Bouwman. A framework for global river flood risk assessments, Hydrol. Earth Syst. Sci., 17, 5, 1871-1892, 2013.

Winter, T. C.: The Vulnerability of Wetlands to Climate Change: A Hydrologic Landscape Perspective, JAWRA Journal of the American Water Resources Association, 36, 305-311, 10.1111/j.1752-1688.2000.tb04269.x, 2000.

Winter, T. C., J.W. Harvey, O.L. Franke, and Alley, W. M.: Ground Water and Surface Water: A Single Resoure, U.S. Government Printing Office, Washington, DC., 1998.

Woznicki, S. A., Baynes, J., Panlasigui, S., Mehaffey, M., and Neale, A.: Development of a spatially complete floodplain map of the conterminous United States using random forest, Science of The Total Environment, 647, 942-953, https://doi.org/10.1016/j.scitotenv.2018.07.353, 2019.

Wu, Q., Lane, C. R., Wang, L., Vanderhoof, M. K., Christensen, J. R., and Liu, H.: Efficient Delineation of Nested Depression Hierarchy in Digital Elevation Models for Hydrological Analysis Using Level-Set Method, JAWRA Journal of the American Water Resources Association, 55, 354-368, 10.1111/1752-1688.12689, 2019a.

Wu, Q., Lane, C. R., Li, X., Zhao, K., Zhou, Y., Clinton, N., DeVries, B., Golden, H. E., and Lang, M. W.: Integrating LiDAR data and multi-temporal aerial imagery to map wetland inundation dynamics using Google Earth Engine, Remote Sensing of Environment, 228, 1-13, https://doi.org/10.1016/j.rse.2019.04.015, 2019b.

1399 Xi, Y., Peng, S., Ducharne, A., Ciais, P., Gumbricht, T., Jimenez, C., Poulter, B., Prigent, C., Qiu, C.,

1400    Saunois, M., and Zhang, Z.: Gridded maps of wetlands dynamics over mid-low latitudes for 1980–2020

1401    based on TOPMODEL, Scientific Data, 9, 347, 10.1038/s41597-022-01460-w, 2022.

1402 Yamazaki, D., S. Kanae, H. Kim and T. Oki. A physically based description of floodplain inundation

1403    dynamics in a global river routing model, Water Resources Research, 47, 4, 2011.

1404 Yamazaki, D., Ikeshima, D., Sosa, J., Bates, P. D., Allen, G., and Pavelsky, T.: MERIT Hydro: A high-

1405    resolution global hydrography map based on latest topography datasets, Water Resources Research, 55,

1406    5053-5073, 10.1029/2019wr024873, 2019.

1407 Zanaga, D., Van De Kerchove, R., De Keersmaecker, W., Souverijns, N., Brockmann, C., Quast, R.,

1408    Wevers, J., Grosu, A., Paccini, A., Vergnaud, S., Cartus, O., Santoro, M., Fritz, S., Georgieva, I., Lesiv,

1409    M., Carter, S., Herold, M., Li, Linlin, Tsendbazar, N.E., Ramoino, F., Arino, O.: ESA WorldCover 10

1410    m 2020 v100, https://doi.org/10.5281/zenodo.5571936 2021.

1411 Zedler, J. B. and Kercher, S.: Causes and consequences of invasive plants in wetlands: Opportunities,

1412    opportunists, and outcomes, Critical Reviews in Plant Sciences, 23, 431-452, 2004.

1413 Zhang, X., L. Liu, T. Zhao, X. Chen, S. Lin, J. Wang, J. Mi and W. Liu. GWL_FCS30: global 30 m

1414    wetland map with fine classification system using multi-sourced and time-series remote sensing

1415    imagery in 2020. Earth Syst. Sci. Data 15, 265-293, 2023.

1416 Zhu, Y., Xu, Y., Deng, X., Kwon, H., and Qin, Z.: Peatland Loss in Southeast Asia Contributing to U.S.

1417    Biofuel's Greenhouse Gas Emissions, Environmental Science & Technology, 10.1021/acs.est.2c01561,

1418    2022.

1419